Mechanical Investigation of Damage in Ligaments

Zheying Guo

Dissertation submitted to the Faculty of the

Virginia Polytechnic Institute and State University

in partial fulfillment of the requirements for the degree of

Doctor of Philosophy

in

Engineering Mechanics

Raffaella De Vita, Chair

Romesh C. Batra

Scott W. Case

Mark A. Stremler

Joseph W. Freeman

May 3, 2011

Blacksburg, Virginia

Keywords: Ligament, MCL, Damage, Subfailure, Constitutive model, Tensile test, SEM

Mechanical Investigation of Damage in Ligaments

Zheying Guo

(ABSTRACT)

Sprains are the most common injuries to ligamentous tissues. They are classified as first-degree, second-degree, or third-degree sprains depending upon their severity. First-degree sprains are the result of over-stretching of ligaments. Second-degree sprains involve partial tears of the ligaments. In third-degree sprains, the ligaments are completely torn. Although first- and second-degree sprains are not as severe as third-degree sprains, they occur more frequently. The mechanisms leading to sprains are still not well understood. Therefore, histo-mechanical experiments and theoretical studies are needed to advance our current knowledge on the etiology of sprains.

In the first part of this study, a structurally-based constitutive equation is proposed to simulate the damage evolution process in ligaments. The ligament is modeled as a bundle of crimped collagen fibers that are assumed to be oriented along one direction, the physiological loading direction. The gradual straightening of collagen fibers determines the nonlinearity in the toe region of the tensile axial stress-strain curve. Straight collagen fibers behave as a linear elastic material. The gradual damage of collagen fibers determines the nonlinearity in the failure region of the tensile axial stress-strain curve. The parameters in the constitutive equation are estimated by curve fitting experimental data on rat medial collateral ligaments (MCLs) published in the biomechanics literature.

In the second part of this study, mechanical experiments are performed in order to identify and quantify damage in ligamentous tissues. MCLs, which are harvested from Sprague-Dawley (SD) rats, are subjected to displacement controlled tensile tests. Specifically, the ligaments are stretched to consecutively increasing stretch values until their complete failure occurs. The elongation of the toe region and decrease in tangent modulus of the linear region of the collected stress-strain data are analyzed and two significantly different damage threshold strains are determined. The effect of age and skeletal maturation on the damage evolution process is also investigated by performing mechanical tests on MCLs isolated from two age groups of SD rats.

In the third part of this study, scanning electron microscopy (SEM) is used to determine variations in the microstructure of ligaments that are associated with the elongation of the toe region and decrease in tangent modulus of the linear region of the stress-strain curve. MCLs from SD rats are subjected to different threshold strains that produce damage and, subsequently, examined using SEM. By comparing the morphology of collagen fibers and fibrils in undamaged and damaged MCLs, the microscopic variations induced by strain are determined and correlated to the observed macroscopic mechanical damage.

Acknowledgments

My first and most earnest acknowledgement must go to my advisor, Dr. Raffaella De Vita, not only for her inspiring ideas and constructive advices that enable me to complete this research, but also her encouragement when it was most needed, not to mention her patience in reading and revising drafts of my dissertation and papers. In every sense, none of this work would have been possible without her guidance.

Many thanks to my committee members: Dr. Batra, Dr. Case, Dr. Stremler and Dr. Freeman, for their comments and suggestions on my research.

I would like to thank Dr. Barrett for help in getting animal samples and Kathy Lowe for her help with the SEM analysis. I am thankful to Jeffrey Twigg and Jeffrey Morelli for their assistance with the experiments. I would also like to thank my friends in the Mechanics of Soft Biological Systems Lab and Department of Engineering Science and Mechanics for the help they provided. Moreover, I thank all my friends for their support over these years.

Finally, my special gratitude goes to my dear parents for their love and support throughout my life.

Contents

List of Figures

Chapter 1

Introduction

1.1 Motivation

Ligaments are fibrous bands of connective tissue, which hold bones together at the joints and support internal organs. The ligaments in the joints serve in guiding their movement, maintaining their stability and restraining their abnormal motion. In the knee joint, which is the largest and most complex joint in the human body, there are four major ligaments: anterior cruciate ligament (ACL), posterior cruciate ligament (PCL), medial collateral ligament (MCL) and lateral collateral ligament (LCL) (Figure 1.1). The MCL and LCL help to stabilize the knee joint by restraining the extension of the knee and preventing the abnormal motion to the inner and outer sides of knee. The ACL and PCL maintain the stability of the knee joint by restraining the forward and backward motion of the knee and limiting its

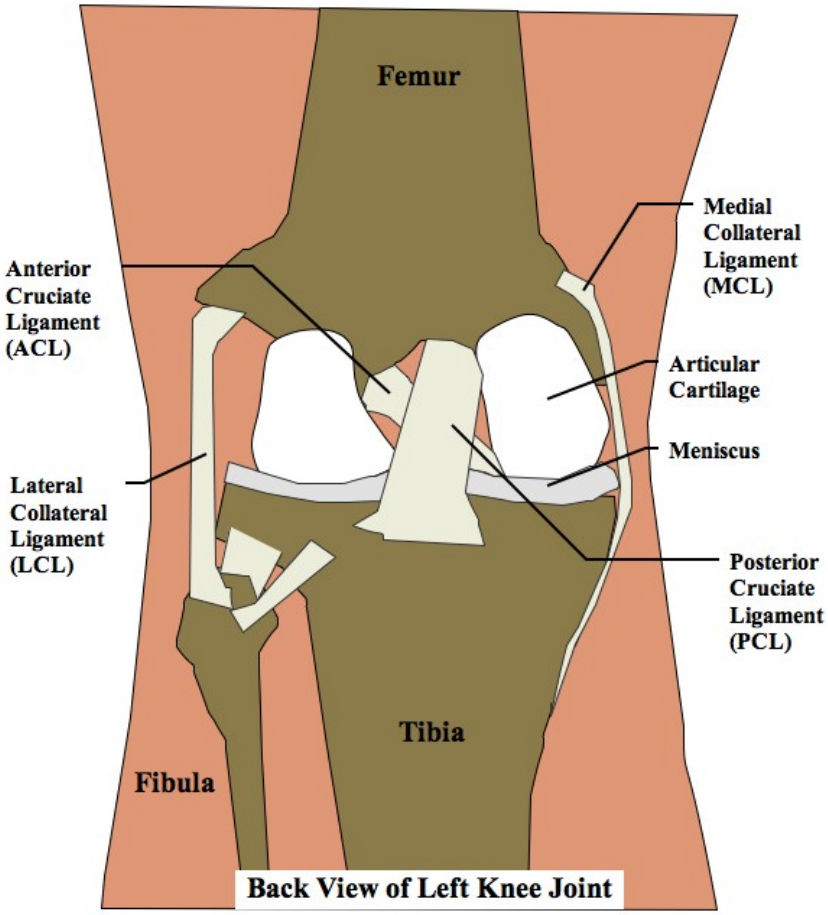

Figure 1.1: Knee joint and its major ligaments.

abnormal rotation.

Injuries to ligaments occur frequently during sport and recreational related activities [2–12]. Peterson et al. [4] investigated the incidence of injuries in football players and reported that the most of the injuries are ligament sprains (around 50%). Hootman et al. [13] compared the NCAA injury data for 15 sports and concluded that the ankle ligament sprains accounted for 15% of all reported injuries. A study by Agel et al. [8] on ACL sprains in NCAA basketball and soccer showed that the injury rates of male soccer players and basketball players were

0.11 and 0.08 per 1000 players per game, respectively, while in female players they were about 3 times higher.

The MCL and ACL were reported to be the most injured ligaments of the knee joint [3, 12, 14]. A study on injuries in ski indicated that ACL and MCL sprains were around 1.25 per 1000 skiers [3]. Miyasaka et al. [2] found that 90% of injuries in knee ligaments were MCL and ACL sprains. Moreover, Hashemi et al. [10] estimated that 100,000 ACL sprains occur every year in the United States. The injuries to MCLs were reported to be 0.24 per 1000 people per year in the United States by Daniel et al. [7].

Sprains are classified by their severity into three degrees: the first degree sprain is an over-stretch of the ligament; the second degree sprain is a partial tear of the ligament; and the third degree sprain is a complete tear of the ligament [15]. It has been reported that 85% of the ligament sprains are first and second degrees sprains [16]. These subfailure injuries not only introduce damage in the ligamentous tissues but produce also laxity in the joint thus compromising its overall stability. The instability in the joint can, on the other hand, cause injuries to other ligaments and tissues. For example, Van de Velde et al. [17] investigated the effect of ACL deficiency on the in vivo elongation of collateral ligaments. They reported that ACL deficiency introduced a great elongation of MCL. Similarly, in an another study on the effect of ACL deficiency on the forces in the tissues of the knee it was shown that the force in the MCL and posterolateral structures significantly increased (up to 413% of the force in an intact knee) in a knee with ACL deficiency [18]. Oates et al. [19] found that the knee injury rate in the ACL-deficient knee is 6.2 times higher than the knee injury rate in

the intact knee.

The financial and time costs required for the treatment of injured ligaments are high. For instance, one epidemiological study reported that an ACL reconstruction costs approximately $17,000 and indicated that the total cost of these reconstructions in the United States amounts to several hundred million dollars [20]. The rehabilitation after surgery usually takes at least 4-6 months [21].

Micro-mechanical studies can provide important information regarding the damage initiation and propagation in ligaments. Thus, they can help in developing novel strategies for the prevention of sport- and recreational-related injuries and improving the current treatment and rehabilitation methods including the development and application of allograft and autograft in surgical reconstructions. *The focus of this dissertation is on understanding and quantifying the mechanical factors that lead to injuries in ligaments.*

1.2 Ligament Morphology

Due to their fibrous structure, ligaments can be regarded as composite materials in which the so-called ground substance is reinforced by collagen and elastin fibers. Collagen is the major component in ligaments acting as the main tensile load carrier (Figure 1.2). Specifically, collagen type I is the main collagen type in ligaments comprising 70%-80% of the ligament dry weight [22, 23]. The amount of elastin fibers is small in ligaments constituting less than 1% of their dry weight.

Collagen in ligaments exists in the form of collagen fibers, which have a hierarchical structure (Figure 1.2). Each collagen molecule, or tropocollagen, is composed of three α-chains, which are amino acid sequences. The diameter of the collagen molecule is about 1.5 nm. Five collagen molecules form a microfibril of approximately 3 nm diameter. In turn, microfibrils aggregate into a subfibril, which has a diameter of 10-20 nm. A group of subfibrils becomes a 50-500 nm diameter fibril through an overlap of molecules, which generates a 64 nm periodicity (D-period). Finally, fibrils form a collagen fiber of 50-300 μm diameter. The collagen fibers form parallel bundles that insert into the bones they are connecting through fibrocartilage and calcified fibrocartilage zones [22]. The fibers appear to be undulated with different crimp patterns when the ligament is unloaded (Figure 1.3). The crimp gradually disappears as the ligament is subjected to loading along the fibers' direction.

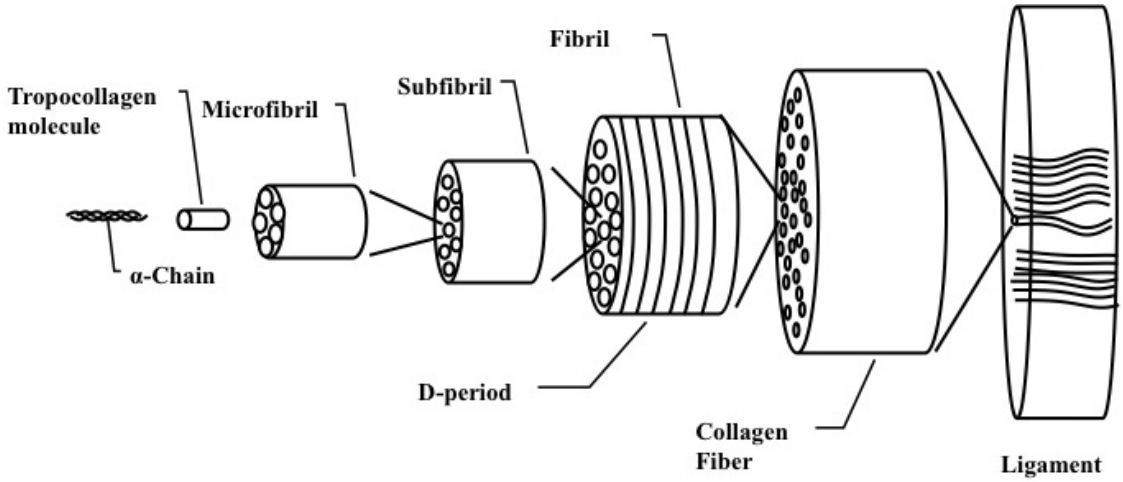

Figure 1.2: Schematic of the hierarchical structure of ligaments.

The ground substance in ligaments acts like a matrix in composite materials. The major

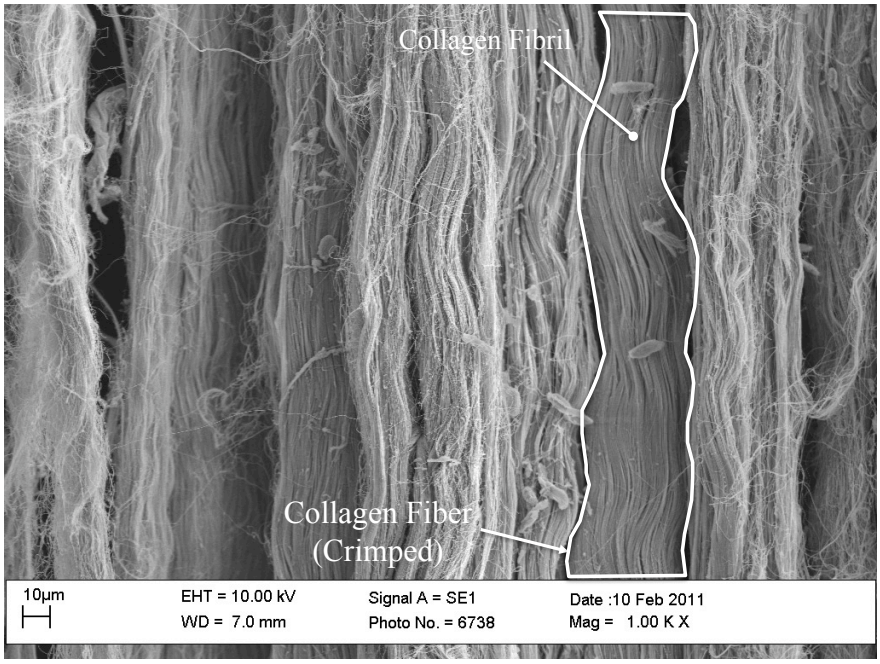

Figure 1.3: SEM picture of crimped collagen fibers.

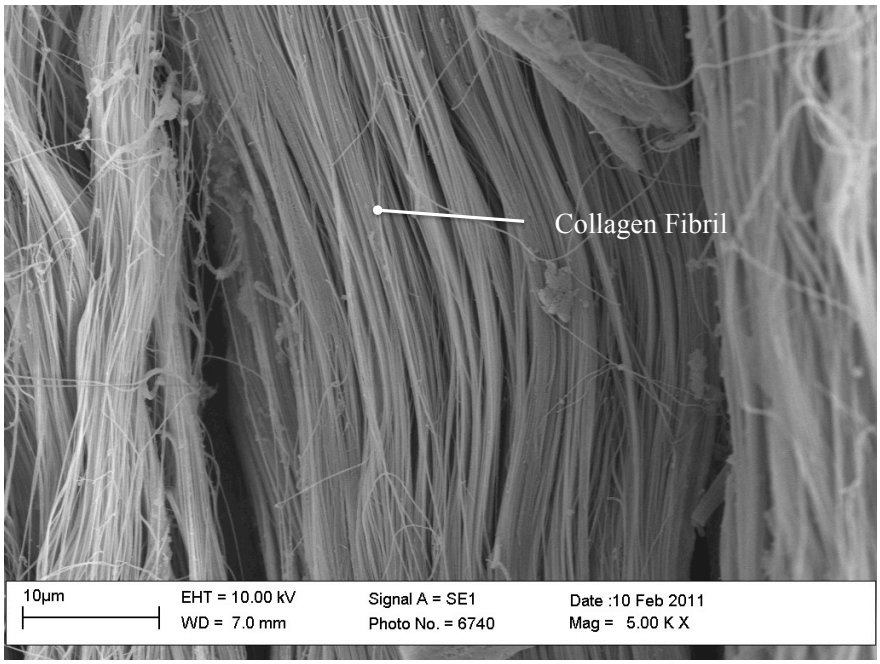

Figure 1.4: SEM picture of collagen fibrils inside a collagen fiber.

component of the ground substance is water (60%-80% of ligament total weight). It also contains proteoglycans and other proteins [22, 24]. The ground substance is considered to be responsible for the viscoelastic behavior exhibited by the ligaments due to its water content [22].

1.3 Tensile Experiments of Ligaments

1.3.1 Typical Nonlinear Stress-Strain Curve

The mechanical properties of ligaments have been mainly investigated by means of uniaxial tensile tests. The typical axial stress-strain (or load-deformation) curve obtained by subjecting ligamentous tissues to these tests is nonlinear with three distinct regions: toe region, linear region and failure region (Figure 1.5). The first nonlinear region is called the toe region. In this region, the slope of the stress-strain curve is initially low and gradually increases. It is believed that the nonlinearity in the toe region is determined by the waviness and gradual recruitment of collagen fibers [22]. As the tensile load increases, the collagen fibers gradually lose their waviness and contribute to support load so the overall slope of stress-strain curve increases. When most of the collagen fibers are straight, the slope of the stress-strain curve becomes constant and the ligament displays a linear behavior. The third nonlinear region of the stress-strain curve is the failure region, which is determined by the failure of collagen fibers.

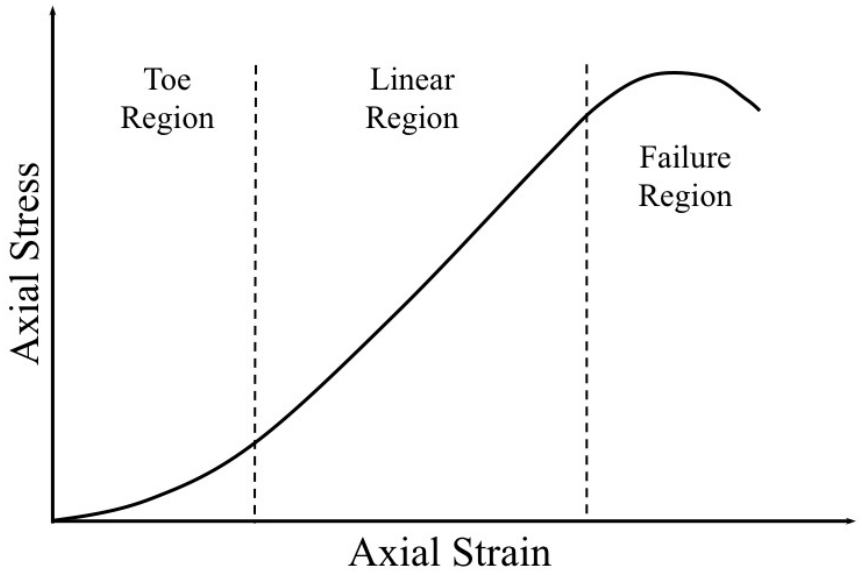

Figure 1.5: Typical axial stress-strain curve for ligaments.

1.3.2 Gripping Methods

One of the challenges encountered in performing mechanical testing of ligaments is clamping of the specimens. Connective tissues placed into regular mechanical grips tend to slip out due to the low friction between the grips and tissue's surface. Moreover, they often break inside the grips. For small animals such as rats and rabbits, the entire bone-ligament-bone complexes of joints are often tested so that the ligaments can be gripped by means of the bones. For example, when testing the mechanical properties of knee ligaments from small animals, the femur and tibia are either mounted on mechanical grips [25, 26] or put into custom-designed molds and then fixed with bone cement [27–29], gypsum plaster [30], or polyester resin [31, 32]. In order to simulate in-vivo physiological conditions, the femur and tibia are oriented in their anatomical position since large differences in mechanical properties

can be observed when varying their orientation [33]. Studies on rabbit MCL [28] and rat MCL [34] indicated, for example, that the MCL is loaded in its anatomical position when the flexion angle between femur and tibia is kept at 70-degree.

1.3.3 Determination of Stress and Strain

Stress-strain data are used to describe the mechanical behavior of ligamentous tissues. The nominal stress, load per unit reference area, is usually reported in tensile axial stress-strain data due to difficulties in measuring the changes in cross-section during testing. In the experiments, the load is measured by the load cell of the tensile testing device. The dimensions of the cross-section of the specimen are measured by contact method such as caliper [29, 35] or non-contact methods such as laser micrometer [26, 36], ultrasonography [37], or laser profile method [38, 39]. The cross-sectional area of the specimen is then computed by making simplifying assumption on its geometry. For example, the cross-sectional area of MCLs is assumed to be rectangular [35] or elliptical [1].

Various techniques are employed for measuring the strain field in ligaments. Contact techniques such as mercury strain gage [40–42] and Hall-effect strain transducer [43, 44] were used in the past. More recently, non-contact strain measurements have been preferred since they do not influence the outcome of the mechanical tests. Video dimension analyzer systems [25, 26] and video motion analysis systems [1, 32, 36, 45], which are based on the use of video systems to track the motions of particles/markers placed on the ligament's surface,

are currently employed to determine the strain field during mechanical testing.

1.3.4 Other Factors that Influence Tensile Properties

There are many factors such as age, sex, hydration of the ligaments that affect the outcome of mechanical tests. For example, experiments on ligaments harvested from animals of different age demonstrated that age and skeletal maturation affect their stiffness [46–48], load at failure [46, 49], energy at failure [46] and mode of failure [48]. Woo et al. [48] showed that femur-MCL-tibia complexes from male rabbits have higher stiffness and ultimate load than those from female rabbits of the same age. Moreover, because the ligaments contain large amount of water (60%-80% of ligament total weight), dehydration during mechanical testing can significantly alter the results of the experiments.

1.4 Literature Review

1.4.1 Review of Mechanical Experiments for Damage in Ligaments

Several experimental studies have quantified and defined damage induced by mechanical stimuli in ligaments. In connective tissues damage produced by fatigue associated with normal daily activities has been studied by several investigators [50–53].

King et al. [50] performed cyclic load relaxation tests on rabbit MCLs and observed a decrease in cyclic peak load of 0.26% per hour. The toe region of the load-deformation curve was also found to increase. The authors speculated that the decrease in peak load was caused by the micro-damage within the ligaments, and the changes in the load-deformation curve were due to changes in the matrix or tissue hydration.

Pollock et al. [51] studied the effect of repetitive strains on the mechanical properties of human glenohumeral ligaments. They observed a non-recoverable increase of residual length and decrease of normalized peak load, which were considered the result of damage accumulation. The residual length and decrease of normalized peak load were found to increase with the applied strain.

Thornton et al. [52] showed that when performing fatigue tests the tangent modulus of rabbit MCLs, which was measured in the upper 50% of the loading curves, decreased. This decrease in tangent modulus was interpreted as an indicator of damage. Decreased residual strength and increased strain in the toe region, which was defined as the strain at 10 MPa stress, observed when monotonically loading the specimens after fatigue tests were reported and attributed to the rupture of collagen fibers. The authors stated that the reduction in tangent modulus during the monotonic loading was a suitable damage marker for fatigue tests.

Recently, Zec et al. [53] studied damage accumulation on rabbit MCLs by conducting fatigue tests. In their study, they measured three different quantities: the tangent stiffness (the slope of the linear region of the load-displacement curve), the secant stiffness (the slope of the line that connects the initial point at 0 mm displacement and the point at the peak

cyclic displacement of the load-displacement curve), and the chord stiffness (the slope of the line connecting the point at 0.1 N load and the point at the peak cyclic displacement of the load-displacement curve). The secant stiffness decreased during cyclic loading while the tangent and chord stiffness were relatively constant. The results of the tests indicated that there was an elongation of the toe region during cyclic loading, which was considered to be due to the failure of short fibers. The authors concluded that a change in the secant stiffness was a better measure of damage than the commonly used change in the tangent stiffness.

In the above-cited studies, damage was evaluated by performing fatigue tests on ligaments and, hence, was the result of events that occurred over a long period of time. There have been a few studies that focused on determining damage from monotonic loading, which is more suited to simulate sprains. Laws et al. [54] studied the histological and mechanical properties in sheep MCLs with second-degree sprains. The ligaments were partially torn by laterally rotating the tibia around pins placed in the tibia. After injury, the ligament was stretched up to failure. A significant increase in joint lateral rotational laxity and valgus laxity together with a reduction in strength by 13.3% were observed.

Panjabi et al. [27, 31] performed tensile tests on rabbit ACLs by loading the specimens to a subfailure deformation defined as 80% of the failure deformation at both high ($\sim$1 m/s) and low ($\sim$1 mm/s) deformation rates. They found that the toe region of the resulting load-deformation curve was more elongated after the subfailure deformation. Structural properties, namely deformation at failure and energy absorbed at failure, were greater in tests conducted at higher deformation rate than in tests conducted at lower deformation

rate.

Lee et al. [55] applied subfailure strains, which were defined as 56% of failure strains, to rat cervical facet capsule ligaments. Although the selected subfailure strain produced a cellular response and pain symptoms in previous research, it was found not to produce structural damage in this study.

Recent studies [1, 56, 57] have focused on elucidating the cellular and micro-structural origin of mechanical damage in rat MCLs. Provenzano et al. [1] studied the effect of subfailure stretches on the tensile properties of ligaments. They reported that the changes in the toe region and linear region of the stress-strain curve increase as the value of the subfailure stretch increases. In their work, structural damage was defined as the increase in non-recoverable strain during a second stretching of the ligaments. By applying different stretches to different MCL specimens and analyzing the damage data, they demonstrated that structural damage occurred at 5.14% strain. Moreover, cellular damage was defined as cell necrosis observed while stretching the tissue.

More recently, by utilizing a polarized light imaging technique combined with tensile testing, Quinn et al. [56, 57] studied damage initiation and its relationship to collagen fiber's arrangement. According to these investigators, damage occurred when changes in the fibers' alignment were detected at 51% of the displacement at failure of the ligaments. However, in this study the ligaments were only stretched to failure and were not subjected to additional loadings as done by other investigators [1, 27, 31, 55]. Additional studies are needed to completely establish the relation between fibers' alignment and damage in ligaments.

1.4.2 Review of Constitutive Models for Damage in Ligaments

Mechanical experiments on ligamentous tissues are, in most cases, costly and require the sacrifice of many laboratory animals. Theoretical models with predictive capabilities are often used for guiding the design of the experiments thus reducing their cost and sacrifice of animals. Moreover, robust theoretical models can offer important information on the mechanical behavior of these tissues, which can be difficult to obtain experimentally.

Theoretical models that describe the damage evolution process in ligaments can be classified into micro-structural models, which are formulated by considering the fine structure of ligaments, and phenomenological models, which are formulated by glossing over their fine structure. One important structural feature of ligamentous tissue is the crimp pattern of the comprising collagen fibers in the unloaded configuration (Figure 1.3). This crimp disappears as the tissue is loaded along the fibers' direction. In several structural models, the straightening process of the collagen fibers is assumed to be responsible for the nonlinearity in the toe region of the tensile stress-strain curve. [58–65].

Kwan and Woo [58] assumed in their model for the tensile behavior of the ligament that the waviness of parallel collagen fibers disappeared at different strain values. The undulated fibers comprising the ligament were divided into m groups: in each group the fibers had equal length and, thus, became taut at the same strain. Each taut fiber was considered to be linear elastic. In order to describe the nonlinear failure region, the fibers were divided into n groups: each group was characterized by having the same failure strain. By dividing

the fibers into m groups with different straightening strains and n groups with different failure strains, the nonlinearity in the toe and failure regions of the stress-strain curve were reproduced.

In the model presented by Hurschler et al. [59, 60], the straightening process of undulated collagen fibers was assumed to be governed by the Weibull distribution. The fibers were aligned in different directions defined by the von Mises distribution. Upon straightening, the collagen fibers were assumed to have a linear elastic constitutive law and fail at the same stretch measured with respect to straightened configuration.

Wren and Carter [61] took into account the contribution of the ground substance in their proposed micro-structural model. The collagen fibers in the tissue were assumed to have different straightening strains and different initial orientation. The nonlinearity of the tissue was attributed to the recruitment of crimped fibers, rotation of fibers in the ground substance, and resistance offered by the ground substance. Each fiber was assumed to become taut and fail at the same straightening and failure stretches, respectively. Moreover, each fiber was assumed to be linearly elastic. The fiber stress in a given direction was computed by averaging the stresses of all the fibers in such direction. The ground substance was assumed to be linear elastic with a defined elastic modulus, failure strain and volume fraction.

Liao and Belkoff [62] assumed that the collagen fibers were arranged in parallel when formulating their micro-structural model for ligaments. The initial lengths of the fibers were randomly defined according to a Gaussian distribution. In order to describe failure, the fibers were assumed to fail at the same stretch relative to their initial length. The model fit

well the stress-strain data which had an abrupt failure region but not the stress-strain data with a gradual and prolonged failure region.

De Vita and Slaughter [63] recently presented a three-dimensional constitutive model for ligaments in which different straightening stretches and different failure stretches were assigned to the collagen fibers. The straightening stretches of the fibers were randomly generated by a Weibull distribution. The straight fibers were assumed to have the same linear elastic stress-stretch relation. The failure stretches were randomly generated by a different Weibull distribution. The anisotropy of the tissues was also modeled by incorporating the different orientation of the fibers.

In the three-dimensional finite strain damage model of Rodríguez et al. [64, 65], damage was attributed to both the matrix and the collagen fibers. The damage of the isotropic matrix was described by adding a damage factor to the strain energy function of the matrix. This damage factor was then defined phenomenologically by using two parameters. The fibers were assumed to have different straightening lengths described by a Beta distribution and damage in each fiber was controlled by its strain energy at failure. Fibers' orientation was also considered. Mullins effects and stiffness reduction that characterized damage were described by the model.

Phenomenological models have been recently proposed to describe damage in ligaments. Arnoux et al. [66] presented a thermodynamically based continuum model for damage of knee ligaments. A damage mechanism was introduced into the model by adding a parameter that produced a reduction in the viscous potential energy.

Pena et al. [67] developed a constitutive model for damage that was based on the assumption that the ligaments were incompressible hyperelastic materials. The damage of collagen fibers and matrix were considered uncoupled. Unlike Rodríguez et al.'s work [64], the authors assumed that the damage behavior of the fibers and the matrix were described by the same phenomenological equation.

Schwab et al. [68] introduced a continuum damage model to describe the results of fatigue and creep tests. Damage was defined as a decrease in the ratio of the cross sectional area of the ligament that still supports load and its initial cross sectional area. The predictions of damage due to fatigue and creep were obtained. However, while the model fit to creep data was good, the prediction of fatigue data was not equally good. Indeed, the fatigue time-to-rupture was overestimated.

Natali et al. [69] presented a visco-hyperelastic constitutive model for damage in ligaments. The model was based on a Helmholtz free energy function depending on the strain history, which is determined by Zener's model. The global damage function was formulated by defining damage parameters on the viscous branch and elastic branch in Zener's model. The model could accurately predict the damage behavior at different strain rates. Ciarletta and Ben Amar [70] formulated a constitutive model based on a finite dissipative theory. The model considered the interaction between fibers and proteoglycans in the matrix. Damage was assumed to be controlled by strain and to depend on strain rate.

1.5 Conclusions

Mechanical experiments have been conducted and constitutive models have been developed to study damage in ligaments. Mechanical damage in ligaments can be detected as elongation of the toe region and decrease in tangent modulus (or stiffness) of the linear region of the stress-strain (or load-deformation) curve [1, 31, 50–53] in tensile tests. Despite the many studies, the initiation and evolution process that leads to damage in ligaments has not been thoroughly investigated. Recently, Provenzano et al. [1] determined the threshold strain for structural damage in rat MCLs by performing mechanical tests. In their experimental protocol, each specimen was stretched up to one level of strain and potential changes in the collected stress-strain curve were evaluated. They reported a single threshold strain, 5.14%, which indicated the initiation of damage observed as elongation of toe region and decrease in tangent modulus of the linear region of the stress-strain curve. This threshold strain was computed by compiling the results obtained from twenty-five different specimens. New experimental protocols are needed to evaluate the threshold strains for damage more accurately due to the inherent biological variability existing among specimens.

Micro-structural [58, 59, 61–65] and phenomenological [66, 67, 69, 71] constitutive equations have been proposed to describe the damage evolution process in collagenous tissues. These equations could fit the three regions (toe, linear, and failure regions) of the experimental stress-strain curves but were unable to predict the effect of subfailure stretches on such curves. Moreover, the damage functions that appeared in phenomenological constitutive

models [64–67, 69, 71] were defined in an ad-hoc manner and, hence, were not directly related with the structural changes that occur into the tissues during injuries.

Experimentalists speculated about the role of the ligaments' microstructure on the observed mechanical damage phenomena. Theoreticians made different assumptions in formulating constitutive models to capture the experimental observations. However, the intrinsic mechanisms that control the damage evolution process in ligaments are still unknown and need further investigation. Thus the focus of this dissertation is to advance our limited understanding of the mechanisms that lead to injuries in ligaments. In Chapter 2, a structurally-based constitutive equation will be presented to simulate the damage behavior in ligaments as determined by subfailure stretches. In Chapter 3, a novel experimental study will be presented, which aims at quantifying the threshold strains that produce mechanical damage in rat MCLs. By performing scanning electron microscopy studies, the results of the mechanical experiments will be interpreted in light of the morphological variations detected at the collagen fiber- and fibril-levels in Chapter 4. Conclusions and future directions for research will be proposed in Chapter 5.

Chapter 2

Constitutive Model for Damage in Ligaments

2.1 Introduction

As already mentioned in Chapter 1, injuries to ligaments can be classified according to their severity as first-, second-, and third-degree sprains. With a first-degree sprain, the ligament is overstretched but the joint remains stable. A second-degree sprain occurs when the ligament is partially torn and moderately affects the joint stability. A third-degree sprain is the most debilitating ligament injury. It consists of a complete rupture of the ligament and causes severe joint instability. While third-degree sprains are the most severe pathology of ligaments, first- and second-degree sprains are the most common. Indeed, epidemiological

studies have estimated that more than 85% of ligamentous injuries consist of first- and second-degree sprains [16].

Despite their high incidence, few experimental studies have been conducted on ligaments to analyze changes in structural properties [27, 31, 54] and mechanical properties [1] when microtrauma and partial tears occur. Panjabi et al. [27] investigated the influence of subfailure injuries on the structural properties of rabbit anterior cruciate ligaments (ACLs). The ultimate load, ultimate deformation, and energy absorbed at failure were seen not to change profoundly following a subfailure injury defined as 80% of the ultimate deformation of the contralateral control ligaments. The shape of the load-deformation curve, however, was noted to be remarkably different with major changes observed in the toe region. In a follow up study, Panjabi and Courtney [31] found that the same subfailure injury at high speed ($\sim$1m/s) produced an increase in the ultimate deformation.

The most comprehensive study of subfailure damage has been conducted on rat medial collateral ligaments (MCLs) by Provenzano et al. [1]. The authors analyzed the effects of different subfailure stretches on tensile axial stress-strain curve. In their experiments, the specimens were stretched to subfailure stretches by performing tensile tests, unloaded and allowed to recover for a time greater than 300$\times$ duration of the test to avoid a viscoelastic creep-recovery response before being reloaded. After recovery, the specimens were stretched again until complete failure of the specimen occurred. These experiments are different than experiments (e.g., hysteresis and preconditioning) in which the specimens are cyclically loaded and unloaded to the same initial stretch by using the same strain rate. The stress-strain

curves during reloading that followed the creep-recovery were observed to change when the subfailure stretches exceeded a threshold stretch corresponding to 5.14%. The toe region was noted to be elongated while the tangent modulus and the tensile strength were found to decrease with increasing subfailure strain.

Because of the difficulties in studying experimentally the damage evolution process in ligaments, constitutive equations need to be formulated to enhance our understanding of the injury mechanisms and to guide the design of appropriate experiments. Several structural [58, 59, 61–64] and phenomenological [66, 69, 70, 72] constitutive equations have been proposed to describe the damage evolution process in collagenous tissues. All these equations can successfully fit the three regions (toe, linear, and failure regions) of the experimental stress-strain curves while some [64, 66, 70, 72] can also describe other mechanical behaviors that are typical of soft tissues. For example, the finite-strain damage constitutive model proposed by Rodríguez et al. [64] can also reproduce the reduction in stiffness between loading and unloading paths in each straining cycle. The anisotropic elasto-damage constitutive model developed in [72] captures the increase in stiffness at low strain values due to cyclic loading. More recently, Natali et al. [69] and Ciarletta et al. [70] have presented damage constitutive models which also consider the viscoelasticity of soft tissues. However, none of the cited models can predict the effect of subfailure stretches (prolonged toe region, decrease in ultimate stress and tangent modulus) as observed and defined by Provenzano et al. in their experimental studies [1].

In this study [73], a new probabilistic model for damage of parallel-fibered collagenous tissues

is presented. The mechanical response of the tissues is assumed to be determined by that of the collagen fibers comprising the tissue. Damage is defined as a reduction in straight collagen fiber's elastic modulus, which occurs at randomly defined stretches. The proposed model can not only reproduce the toe, linear, and failure regions of the stress-strain curve in ligaments but, unlike previous models, it can also predict the changes in the stress-strain curve such as prolonged toe region, decrease in tensile strength and tangent modulus that are determined by subfailure stretches. The predictive capabilities of the model are investigated by studying the effect of the structural parameters on the tensile behavior of ligaments and by using published tensile data [1].

2.2 Model Formulation

2.2.1 Preliminaries and Basic Assumptions

Ligamentous tissues can be regarded as composite materials consisting of collagen fibers and elastin fibers embedded in a proteoglycan-rich matrix, the so-called *ground substance*. Collagen, which occupies 65%-80% of the total dry weight of ligaments, is the main load carrying component. Elastin constitutes less than 1% of the dry weight of ligaments and is responsible for elastic recovery. Water occupies 60-70% of the tissue's total weight [74].

Collagen has a hierarchical structure: collagen molecules are packed together to form collagen fibrils, collagen fibrils aggregate to form collagen fibers and collagen fibers are arranged in

fascicles [75]. The collagen fibers are wavy when unstrained and gradually lose their waviness under axial strain [76]. Moreover, they exhibit a linear elastic behavior [77].

To describe the tensile behavior of ligaments, a structural one-dimensional model is presented hereafter. In the model formulation, the collagen fibers are assumed to be the only ligaments' component that determines their mechanical behavior. Collagen fibers are assumed to be linear elastic and parallel to the ligaments' loading direction. They are assume to be wavy and gradually become straight and damaged under axial strain. The elastic modulus of each collagen fiber decreases at different damage stretches. The ligament's stress is defined as the average of the stresses of the constituent collagen fibers. Elastin contribution is neglected due to its small amount. Moreover, the ground substance and its interaction with the collagen fibers are ignored.

2.2.2 Collagen Fiber and Ligament Stretch

The ligament is assumed to be made of N parallel collagen fibers, where N is a non-negative integer. The collagen fibers are defined randomly by their straightening stretches according to a Weibull distribution [78]. The Weibull distribution is a one-tailed continuous probability distribution widely used in reliability and life data analysis due to its versatility. It has three-parameters –the so-called shape, scale and location parameters – that can be varied to mimic the behavior of other probability distributions such as, for example, the exponential

distribution. The probability density function (PDF) of a Weibull random variable Λ_s is

$$p(\Lambda_s;\alpha_s,\beta_s,\gamma_s)=\begin{cases}0 & \text{for} \quad \Lambda_s<\gamma_s\,,\\ \frac{\alpha_s}{\beta_s}\left(\frac{\Lambda_s-\gamma_s}{\beta_s}\right)^{\alpha_s-1}e^{-\left(\frac{\Lambda_s-\gamma_s}{\beta_s}\right)^{\alpha_s}} & \text{for} \quad \Lambda_s\geq\gamma_s\,,\end{cases} \tag{2.1}$$

where Λ_s is the fiber's straightening stretch, which is the stretch at which the fiber becomes straight, $\alpha_s>0$ is the shape parameter, $\beta_s>0$ is the scale parameter, and $\gamma_s>0$ is the location parameter. The cumulative distribution function associated with (2.1) is

$$P(\Lambda_s;\alpha_s,\beta_s,\gamma_s)=\begin{cases}0 & \text{for} \quad \Lambda_s<\gamma_s\,,\\ 1-e^{-\left(\frac{\Lambda_s-\gamma_s}{\beta_s}\right)^{\alpha_s}} & \text{for} \quad \Lambda_s\geq\gamma_s\,.\end{cases} \tag{2.2}$$

By inverting equation (2.2) for $\Lambda_s\geq\gamma_s$, one obtains the following relation

$$\Lambda_s(P;\alpha_s,\beta_s,\gamma_s)=\gamma_s+\beta_s[-\ln(1-P)]^{\frac{1}{\alpha_s}}\,. \tag{2.3}$$

Equation (2.3) can be used to generate randomly distributed collagen fibers by generating their associated straightening stretches. Let $\Lambda_s^{(i)}$ be the straightening stretch of i^{th} collagen fiber ($i=1,2,\ldots,N$). Then, $\Lambda_s^{(i)}$ can be defined as

$$\Lambda_s^{(i)}(P_s^{(i)};\alpha_s,\beta_s,\gamma_s)=\gamma_s+\beta_s[-\ln(1-P_s^{(i)})]^{\frac{1}{\alpha_s}} \tag{2.4}$$

where $P_s^{(i)}$ is a random number between 0 and 1.

Let Λ be the overall stretch of the ligament. Each collagen fiber is stretched only after losing its waviness. Thus, the stretch of i^{th} collagen fiber, which is denoted by $\Lambda^{(i)}$, is computed relative to its straightening stretch, $\Lambda_s^{(i)}$, and is defined as $\Lambda^{(i)}=\Lambda/\Lambda_s^{(i)}$.

2.2.3 Damage and Collagen Fiber Stress

Damage is assumed to be a stretch controlled process. The i^{th} collagen fiber possess M damage stretches, where M is a non-negative integer. These stretches are randomly generated by using a Weibull distribution. Thus, by arguments similar to those used to derive equation 2.4, the j^{th} subfailure stretch ($j = 1, 2, \ldots, M$) of the i^{th} collagen fiber is given by

$$\Lambda_d^{(j)}(P_d^{(j)}; \alpha_d, \beta_d, \gamma_d) = \gamma_d + \beta_d[-\ln(1 - P_d^{(j)})]^{\frac{1}{\alpha_d}} \tag{2.5}$$

where $P_d^{(j)}$ is a random number between 0 and 1, $\alpha_d > 0$, $\beta_d > 0$, and $\gamma_d > 0$ are the shape, scale, and location parameter of the Weibull distribution, respectively.

Each collagen fiber is linearly elastic with elastic modulus K. The elastic modulus of the collagen fiber is reduced by a damage reduction factor D ($0 < D < 1$) when damage occurs. This reduction in elastic modulus can be attributed to breakage of fibrils in each collagen fiber. The limit $D = 0$ describes the complete failure of the collagen fiber while the limit $D = 1$ represents the case in which the collagen fiber is not damaged.

Thus, the stress of i^{th} collagen fiber, which is denoted by $\sigma^{(i)}$, is defined as

$$\sigma^{(i)} = \begin{cases} 0 \quad \text{for } \Lambda^{(i)} \leq 1 \quad \text{(i.e. wavy fiber)}\,, \\ K(\Lambda^{(i)} - 1) \quad \text{for } 1 < \Lambda^{(i)} < \Lambda_d^{(j)} \text{(i.e. straight, undamaged fiber)}\,, \\ (D^j)K(\Lambda^{(i)} - 1) \quad \text{for } \Lambda^{(i)} \geq \Lambda_d^{(j)} \text{(i.e. straight, damaged fiber)}\,, \end{cases} \tag{2.6}$$

where $1 \leq j \leq M$ and $\Lambda_d^{(1)} \leq \Lambda_d^{(2)} \leq \cdots \leq \Lambda_d^{(M)}$. It must be noted that D^j denotes the exponentiation with base D and exponent j. Figure 2.1 illustrates an example of stress-stretch curve for a single straight collagen fiber that is damaged $j = 5$ times at five different

stretches, $\Lambda_d^{(1)}$, $\Lambda_d^{(2)}$, $\Lambda_d^{(3)}$, $\Lambda_d^{(4)}$, $\Lambda_d^{(5)}$. In this example, the initial elastic modulus K of the collagen fiber is reduced to $(D^j)K$ at each $\Lambda_d^{(j)}$ and D has been set to be equal to 1/2.

The overall stress of the ligament is defined as the average of the stresses of the N collagen fibers. Thus, it is given by

$$\sigma = \frac{1}{N}\sum_{i=1}^{N}\sigma^{(i)}\,. \tag{2.7}$$

Thus, the tensile behavior of the ligament can be described by (2.4)-(2.5)-(2.6)-(2.7) and, hence, requires the following set of parameters $\{K,\ D,\ \alpha_s,\ \beta_s,\ \gamma_s,\ \alpha_d,\ \beta_d,\ \gamma_d,\ N,$ and $M\}$. Below it will be explained how the number of parameters can be reduced and computed by using experimental data.

2.3 Results

In order to demonstrate the capability of the model, the number N of collagen fibers that constitute the ligament has been chosen to be 10^5. It needs to be noted that this number does not represent the effective number of fibers that occupy the ligamentous substance. Indeed, in the numerical implementation of the model, no differences are noticed in the value of the stress σ defined by (2.7) when the number N is increased beyond 10^5. The number M of damage stretches in straight collagen fibers can be related to the number of fibrils that could break thus producing a reduction in collagen fiber's elastic modulus. M has been set to be 100 since approximately hundreds of fibrils make up a single collagen fiber. The straightening stretches of the collagen fibers and damage stretches of each straight collagen fiber have been

computed by transforming uniform deviates generated by using Park and Miller's Minimal Standard generator with an additional shuffle [79, 80] into Weibull distributed deviates via equations (2.4) and (2.5).

Published experimental data by Provenzano et al. [1] on rat MCLs have motivated the formulation of the proposed model and have been used to validate its predictions. The stress-strain data reported in Figure 5-F of [1] have been digitized and employed to determine the values of the model parameters. The results of the curve fitting performed by minimizing the sum of the squared differences between the predicted and measured values of the ligament's stress via the Differential Evolution code [81] are shown in Figure 2.2. The Differential Evolution is a robust genetic type algorithm that can be used to minimize any kind of function with any kind of constraints defined on continuous, discrete, and mixed search spaces. The values of the material parameters obtained are $K = 1059$ MPa, $\alpha_s = 1.000$, $\beta_s = 0.0273$, $\alpha_d = 2.052$, $\beta_d = 0.2357$, $D = 0.8992$ ($R^2 = 0.99$). These parameters provide a unique minimum in the bounded parameter space defined by the following intervals: $0 \leq K \leq 10000$, $1 \leq \alpha_s \leq 10$, $0 \leq \beta_s \leq 10$, $1 \leq \alpha_d \leq 10$, $0 \leq \beta_d \leq 10$, $0 \leq D \leq 1$. The bounds on the parameters α_s, β_s, α_d, and β_d are set so as to avoid that all the fibers are already straight and the fibrils are already damaged at very small strains. The parameters are computed via the minimization so that they can then be varied for studying the effect of each structural parameter on the overall stress-stretch response. It was assumed that the location parameter, γ_s, of the Weibull distribution that describes the collagen fibers' straightening process is equal to 1. Such assumption is physically sound and implies that the collagen fibers cannot become

straight under compression, i.e. when the axial strain is less than 0. The location parameter, γ_d, of the Weibull distribution that defines the damage stretches of the collagen fiber has been fixed to be 1.0514. This is the stretch value corresponding to the 5.14% strain at which damage occurs in rat MCLs [1].

Due to the lack of combined mechanical and histological experimental data on partial and complete failure of collagenous tissues, the predictive capabilities of the constitutive model have been studied by varying the values of its structural parameters within bounds that are dictated by their physical meaning. The values of the parameters, which are not varied in all these predictions, have been fixed to the values obtained by curve fitting the experimental data published by Provenzano et al. [1]. The effect of different subfailure stretches on the stress-stretch curves of ligaments are illustrated in Figure 2.3. The stress-stretch curve for a ligament obtained during first loading up to a given subfailure stretch is assumed to be equal to the stress-stretch curve of its corresponding contralateral control ligament (up to that subfailure stretch) in agreement with the experiments. The first loading curve in Figure 2.3 is plotted for the values of the material parameters obtained from the curve fitting procedure described above and using the data collected on the contralateral control ligament. The different second loading curves depicted in Figure 2.3 are then predicted by computing how many fibrils are broken in the collagen fibers during the first loading up to subfailure stretches equal to 1.05, 1.1, 1.14, and 1.17. Qualitatively, the changes in stress-stretch curve produced by subfailure stretches are comparable with the experimental data [1] in which damage, which appears for a subfailure stretch higher that 1.0514, was characterized by

a more prolonged toe region and a reduction in tangent modulus of the linear region and ultimate stress. The model was also used to predict the reduction in stress produced by a subfailure stretch of 1.09 as reported in the experimental study by Provenzano et al. [1]. The prolonged toe region and reduction in tangent modulus of the linear region were obtained but the stress values predicted by the model were higher than the experimental stress values (Figure 2.10).

In Figures 2.4 and 2.5, the stress-stretch curves predicted by the model are depicted for various values of the shape parameter, α_s, and scale parameter, β_s, of the Weibull distribution that describes the fiber straightening process. It can be seen that, by changing these parameters, the toe region of the stress-stretch curve changes. As the value of α_s increases, more collagen fibers become straight at a greater stretch, which corresponds to the stretch at which the Weibull PDF has the maximum. The resulting stress-stretch curve has a more prolonged toe region, increased tangent modulus in the linear region, and greater ultimate stress (Figure 2.4). As the value of β_s increases, the Weibull PDF becomes flatter implying that the straightening process of collagen fibers occurs over larger strain intervals since the straightening stretches of collagen fibers are more evenly distributed. Thus, the toe region is also prolonged but both the tangent modulus in the linear region and the ultimate stress decrease since the probability of fibers being straight and, hence, supporting load also decreases (Figure 2.5).

In Figures 2.6 and 2.7, the stress-stretch curve is presented for different values of the shape parameter, α_d, and scale parameter, β_d, of the Weibull distribution that defines the damage

stretches of individual collagen fibers. By varying these parameters, the failure region of the stress-stretch curve changes while the toe region remains unaffected. As the value of α_d increases, the Weibull PDF becomes sharper and its maximum value shifts to the right. This indicates that straight fibers are damaged at larger stretches and sudden failure is more probable. Therefore, greater failure stretch, tensile strength and a sharper stress-stretch curve are associated with a greater value of α_d. As the value of β_d increases, the maximum value of Weibull PDF also shifts to the right but the shape of the Weibull PDF appears to become flatter β_d. This results in greater failure stretch and ultimate strength and more gradual failure process.

In Figure 2.8, the stress-stretch curves are depicted for different values of the damage reduction parameter, D. One can observe that as D increases, the stress sustained by the tissue increases. For a fixed M, high values of D indicate that little damage is produced in straight collagen fibers and, hence, their tangent modulus in the linear region is slightly reduced.

By changing the number of damage stretches in a straight collagen fiber , M, the model can reproduce different failure modes as shown in Figure 2.9. Precisely, for low values of M, the failure region of the stress-strain curve has a more jagged appearance that is often observed during tensile tests. One must also observe that when $M \to \infty$ or $D \to 0$ in (2.6), the current model becomes similar to a previous model that describes complete failure in ligaments [63].

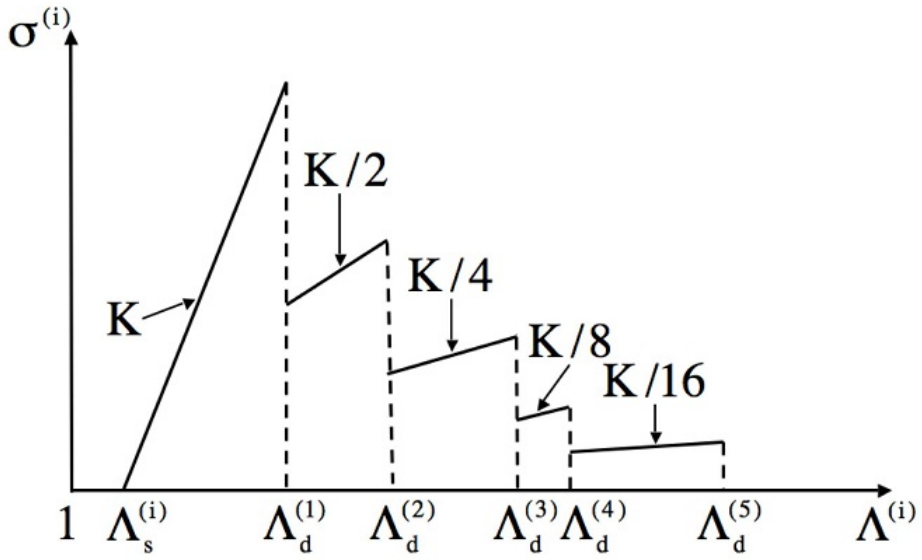

Figure 2.1: Example of stress-stretch relation for the i^{th} collagen fiber. In this example, damage is assumed to occur at five stretches, $\Lambda_d^{(j)}$ with $j = 1...5$, and causes a reduction in elastic modulus by a factor D chosen to be equal to 1/2.

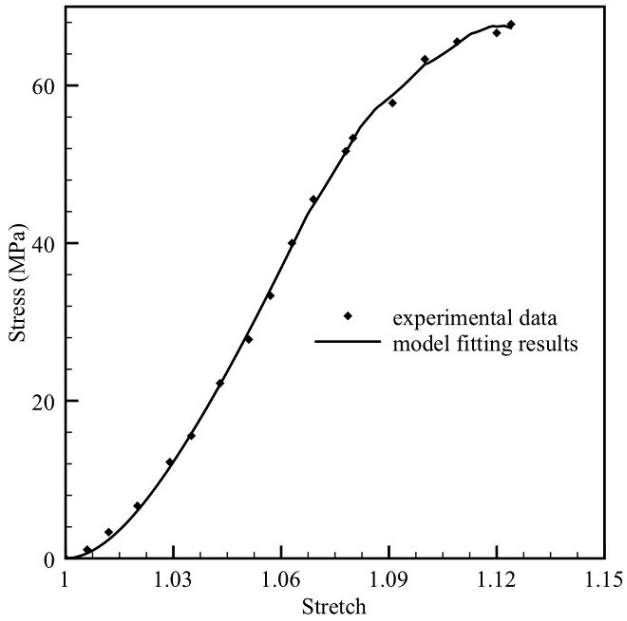

Figure 2.2: Model fit to tensile experimental data.

2.4 Discussion

A novel probabilistic constitutive equation for damage in parallel-fibered collagenous tissues such as ligaments has been formulated. The constitutive equation has been shown to successfully reproduce the stress-stretch curves for rat MCLs (see Figure 2.2) and the changes in such curves determined by subfailure stretches (see Figure 2.3). The only experimental data available in the literature on damage in ligaments [1] have been used to determine the values of six model parameters by using the Differential Evolution algorithm. The fitting parameters have been then varied for analyzing their role on predicting the tensile damage behavior in ligaments.

Determining the values of all the parameters uniquely by curve fitting only one macroscopic

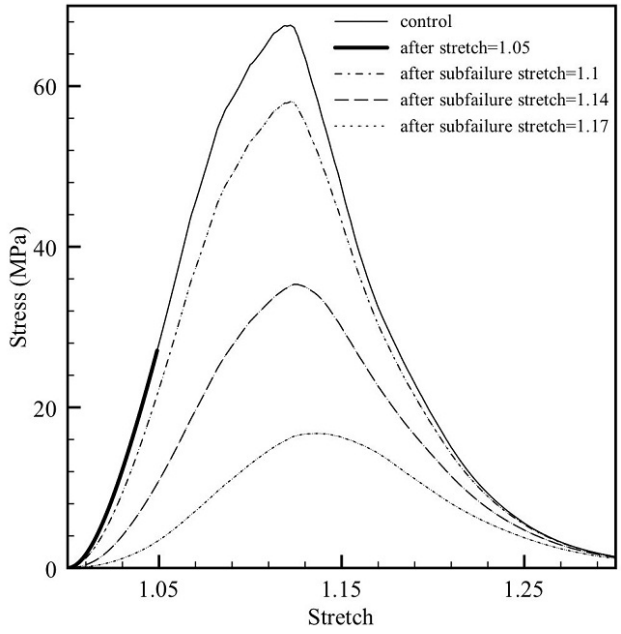

Figure 2.3: Model prediction for different values of subfailure stretches. The first loading curve (continuous line) is plotted for the values of the material parameters obtained from curve fitting. The different second loading curves (bold and dashed lines) are then predicted by computing how many fibrils are broken in the collagen fibers during the first loading up to subfailure stretches equal to 1.05, 1.1, 1.14, and 1.17.

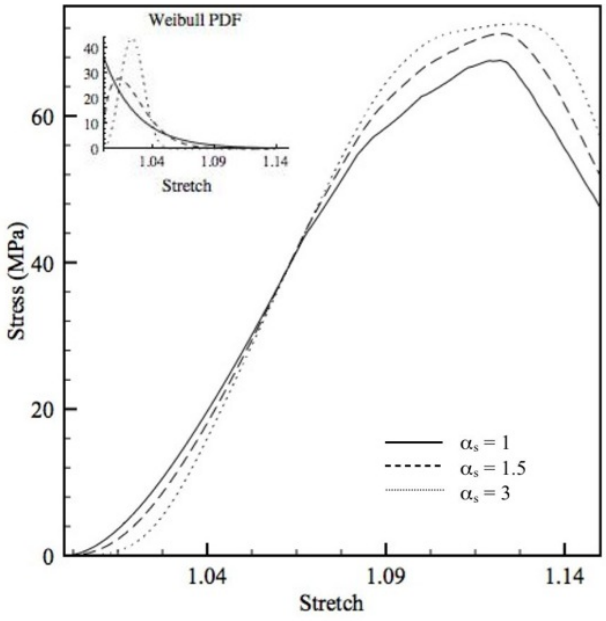

Figure 2.4: Model results and associated Weibull PDF defining collagen fiber straightening process for different values of α_s.

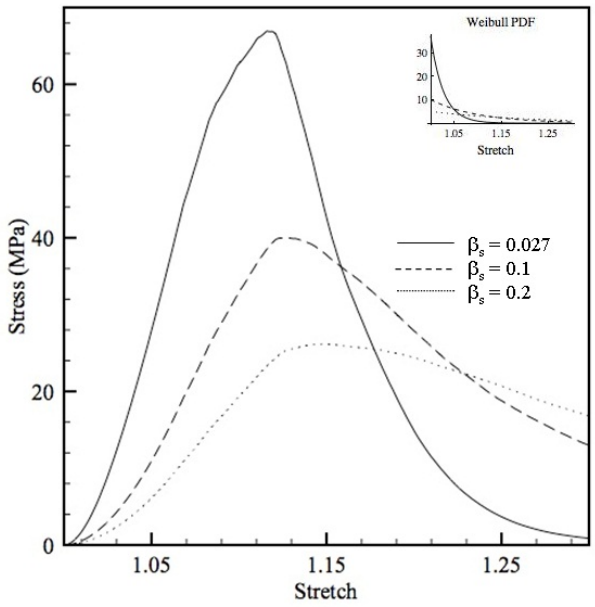

Figure 2.5: Model results and associated Weibull PDF defining collagen fiber straightening process for different values of β_s.

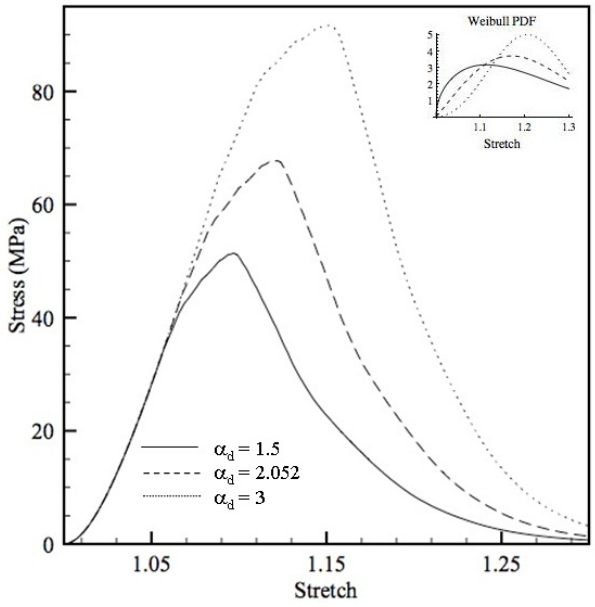

Figure 2.6: Model results and associated Weibull PDF defining collagen fiber damage process for different values of α_d.

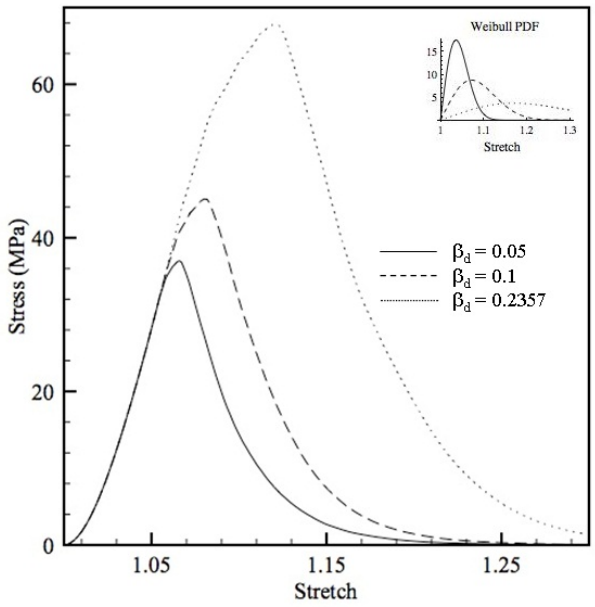

Figure 2.7: Model results and associated Weibull PDF defining collagen fiber damage process for different values of β_d.

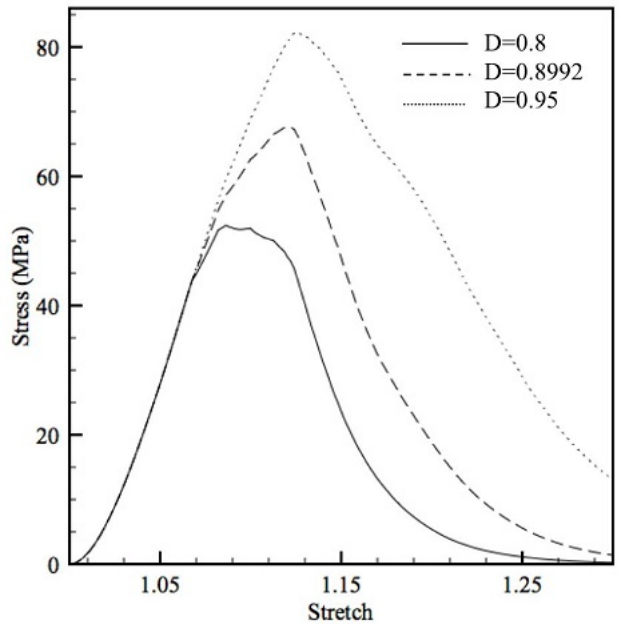

Figure 2.8: Model results for different values of D.

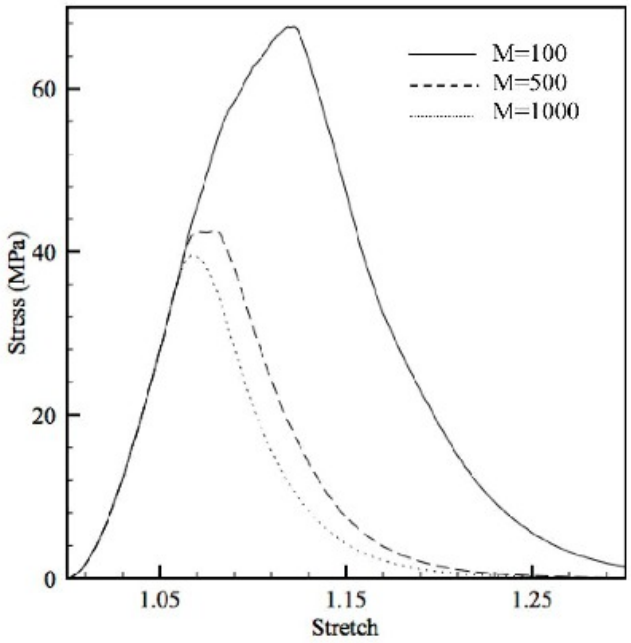

Figure 2.9: Model results for different values of M.

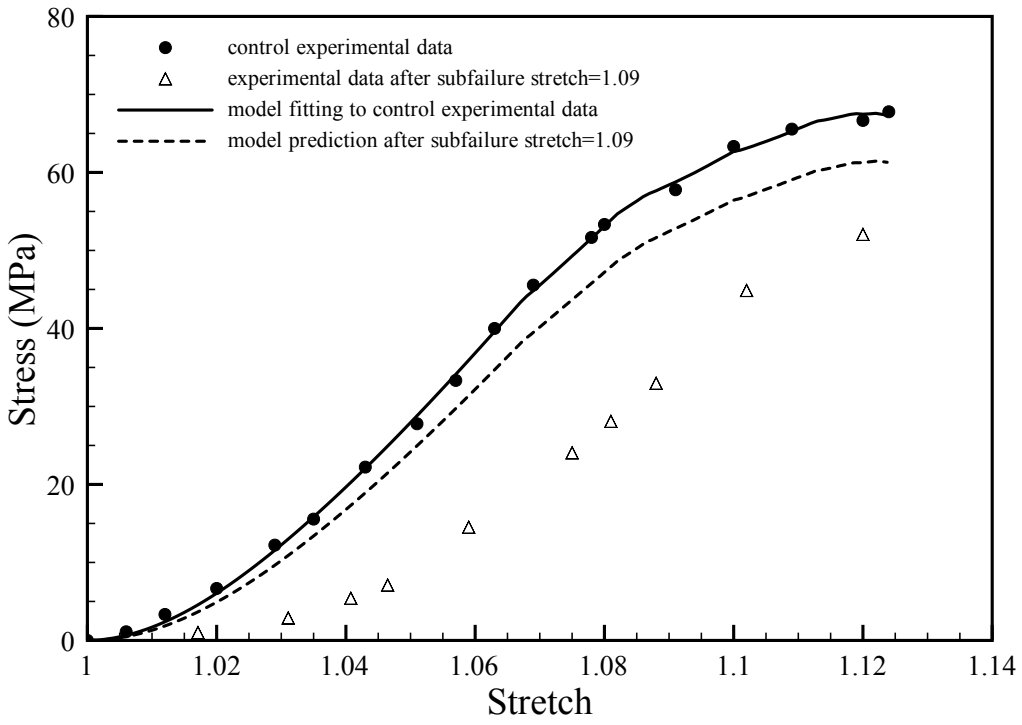

Figure 2.10: Comparison between model prediction and experimental data [1].

stress-strain curve is not possible unless restrictions are imposed on such parameters. However, it is believed that, by combined micro- and macro-experiments, one could determine independently the values of subsets of parameters. Moreover, because the parameters are directly related to the tissue's structure determined by the collagen fibers, they are physically meaningful. Therefore, when finding the parameter values by minimizing the sum of squared residuals, restrictions can be imposed as dictated by their physical significance.

Two Weibull distributions have been selected to randomly generate straightening stretches of collagen fibers and damage stretches in each collagen fiber. These one-tailed distributions have been preferred over two-tailed distributions (e.g. Gaussian distribution) because they do not describe unrealistic scenarios in which collagen fibers are straight, support load, and are damaged when the the axial strain is less than 0. The location parameters of the Weibull distributions have been fixed to reduce the number of model parameters and obtain a locally unique solution via the minimization process. Specifically, γ_s has been set to 1. This assumption implies that every collagen fiber is wavy in the initial configuration. In addition, γ_d was fixed to 1.0514. One must note that this collagen fiber's stretch value corresponds to 5.14% ligament's strain at which damage occurs [1]. However, it is speculated that damage at the collagen fiber level may manifest at a lower strain than damage at the tissue's level and, hence, γ_d may have a lower value than 5.14% .

In the proposed model, the ligament is assumed to be a bundle of parallel collagen fibers having different waviness. The model is different from the fiber bundle model (FBM) used for modeling the failure of fiber reinforced composite materials [82–84]. In the FBM, the fibers

are assumed to be straight and break when the applied stress (or strain) exceeds critical values that are defined using a PDF. The stress of the broken fibers is then carried out by the remaining unbroken fibers using global or local load sharing. In the proposed model, the collagen fibers are damaged only after becoming taut. They do not completely break at critical strain values but their elastic moduli decrease. This failure mechanism increases the capability of the model to predict abrupt and gradual modes of failure experimentally observed in ligaments. A few studies [85, 86] have successfully applied a similar approach to composite materials thus showing that different elasto-plastic tensile responses can be predicted. It must be noted also that, in the proposed model, damage in the collagen fibers was assumed to be determined by the complete failure of the comprising fibrils. The failure of fibrils within each fiber was described by the FBM.

The parameters in the Weibull distributions, $\{\alpha_s, \beta_s, \gamma_s, \alpha_d, \beta_d, \gamma_d\}$ as well as the collagen fiber's elastic modulus, K, and its reduction, D, could be determined by designing appropriate experiments as described hereafter. For example, recent experiments by Hansen et al. [76] have shown that information about the straightening process of collagen fibers can be correlated with tensile stress-strain data by using optical coherence tomography. Hurschler et al. [60] have used the results of the above cited experiments to compute the parameters of a micro-structural model in which the straightening process is also defined by means of a Weibull distribution. They have shown that the location parameter can be uniquely determined when enough experimental data for the toe region of the stress-strain curve are available. The collagen fiber's elastic modulus as well as its reduction due to damage could

be determined by using x-ray diffraction techniques as previously done by Sasaki et al. [77] or, alternatively, by atomic force microscopy.

Three-dimensional constitutive equations are necessary to accurately describe the mechanical behavior of ligaments [87]. Although the proposed model is one-dimensional, one must note that it can be extended to a three dimensional model by using Lanir's structural approach for soft tissues [88] as previously suggested by De Vita and Slaughter [63, 89]. Information on collagen fiber orientation in ligaments and three-dimensional experimental data are needed to finally test a generalized three-dimensional structural model.

More experiments need to be conducted to study the damage evolution in collagenous tissues and evaluate the predictive capabilities of proposed model. The model successfully fits the available stress-stretch data and describes the prolonged toe region, decrease in tangent modulus and ultimate stress observed after subfailure stretches reported for MCLs. However, when used to *predict* the stress after a subfailure stretch corresponding to approximately 9% strain as reported by Provenzano et al. [1] (see Figure 5-F), the computed stresses are overestimated. These predictions could be due to the assumption that collagen fibers are damaged at a stretch equal to 1.0514 when tissue's damage has been reported to occur. However, if collagen fibers are assumed to experience damage at a stretch that is lower than 1.0514, the predicted stresses will have lower values.

The model predictions suggest that other mechanisms such as, for example, breaking of collagen intermolecular cross-links, interfibrillar cross-links, and debonding of fibrils from the proteoglycan-rich matrix need to be incorporated into structural models to accurately

predict damage in ligaments. The shape of the toe region, tangent modulus, and tensile strength of collagenous tissues depend on the presence of collagen crosslinks both at the molecular and fibrillar level [90, 91]. Moreover, the mechanical role of the ground substance needs to be considered since its removal from collagenous tissues causes a decrease in tangent moduli and nominal stresses [92] as observed in damaged ligaments [1]. Finally, according to Screen et al. [93, 94], the proteoglycan content affects the sliding between adjacent collagen fibers believed to be responsible for failure of fascicles.

The proposed model does not account for the short-term and the long-term viscoelasticity experimentally observed in ligamentous tissues. Therefore, it cannot describe viscoelastic phenomena such as the effect of strain rate, hysteresis, creep, and relaxation. To our knowledge, little work has been done in developing constitutive models that can capture both the damage and viscoelasticity of ligaments [69, 70]. Ongoing studies in our laboratory include the development of a structural constitutive model that describes viscoelastic phenomena by assuming that the elastic collagen fibers are embedded in a viscoelastic ground substance.

Chapter 3

Mechanical Experiments of Damage in Ligaments

3.1 Introduction

The majority of ligament injuries are grade I and grade II injuries which are the overstretches and the partial tears of ligament [15]. Damage to ligaments reduces their performance and, consequently, increases the instability of the joint they connect. Hence, injured ligaments may cause further injury to other connective tissues in the joint [95]. Understanding the damage initiation and evolution in ligamentous tissues would help in developing adequate prevention and treatment strategies.

Studies have been carried out on soft tissues to investigate the damage that may occur during

daily activities through fatigue experiments [35, 50, 51, 53, 96–99]. Non-recoverable decrease of cyclic peak load [50, 51] or decrease of stiffness or modulus [52, 96–98], and elongation of the toe region [50–53, 98, 99] associated with increasing cycle numbers were reported in these studies and employed as parameters to evaluate the effect of damage produced by fatigue loading. In these studies, cumulative damage produced by multiple loading cycles was evaluated.

There are a few studies on the effect of monotonic loading of ligaments' damage. This loading emulates better the mechanical condition that produce sprains. Laws et al. [54] produced damage to sheep MCLs by laterally rotating the tibia. They reported significant increase in joint laxity and 13.3% decrease in strength. Panjabi et al. [27, 31] conducted high ($\sim$1 m/s) and low ($\sim$1mm/s) deformation rate tensile tests on rabbit ACLs and loaded the specimens up to a subfailure deformation defined as 80% of the failure deformation. They measured the deformation of the ACLs at different load levels and found that the load-deformation curve was elongated. The stiffness measured at 50% of the failure load also changed after subfailure deformation. Panjabi et al. [100] also compared the effect of a single subfailure stretch and a series of incremental subfailure stretches that ended at the same stretch value on rabbit ACLs. They demonstrated that there is no significant difference in the load-deformation curves and viscoelastic properties that follow from the stretching protocols. Provenzano et al. [1] determined the threshold of damage in rat MCLs. In their study, different subfailure stretches were applied to different MCL specimens with each specimen receiving a single subfailure stretch. The non-recoverable increase in the preload length

of the ligament subjected to subfailure stretch was defined as structural damage. Cellular damage was also studied and associated with cell necrosis. The structural damage data from different experiments at different subfailure stretches was calculated and fit to a linear model to obtain a strain of 5.14% that indicated the onset of damage. Recently, Quinn et al. [56, 57] studied collagen fiber arrangement during tensile testing by using polarized light imaging technique. They detected damage with the change in the fibers' alignment at 51% of the failure displacement. However, the relation between fibers' alignments and the non-recoverable damage of ligament remains unclear.

It has been shown that skeletal maturation and age influenced the mechanical properties of ligaments. The results of tensile tests demonstrated that ligaments of older animals have higher stiffness [46, 47] and failure energy [46] than those of younger animals. Woo et al. [48, 49] investigated the mechanical properties of MCLs from skeletal immature and mature rabbits and concluded that the stiffness, ultimate load and failure energy increased after maturation.

In this paper, the damage evolution process in rat MCLs will be studied by performing displacement-controlled tensile tests at incrementally increasing displacements. The non-recoverable changes in axial stress-strain curves at each loading will be considered as damage phenomena. The link between the damage phenomena and applied strain levels will be analyzed to compute the threshold strains for damage. The proposed experimental protocol permits a more accurate evaluation of threshold strains for damage when compared to other protocols in which the threshold strains were evaluated from different samples subjected to

different stretches [1]. In our study, the effect of skeletal maturation and age on damage will also be investigated by testing MCLs from two age groups of rats.

3.2 Materials and Methods

This study was conducted in accordance with applicable laws, regulations, guidelines, and policies (i.e., the U.S. Animal Welfare Act, Public Health Service Policy, U.S. Government Principles, and the Guide for the Care and Use of Laboratory Animals). All procedures were conducted with approval of the Institutional Animal Care and Use Committee at Virginia Tech. Thirty-two Sprague Dawley male rats of two age groups were purchased from Harlan Laboratories (Frederick, MD). Sixteen rats were 57±1 days old (258.7±7.8 g, body mass) and sixteen rats were 84±3 days old (342.2±15 g, body mass). The rats were euthanatized with 4 ml of Beuthanasia D solution intraperitoneal injection (phenytoin and pentobarbital; each ml: active ingredients: 390 mg pentobarbital sodium, 50 mg phenytoin sodium). Immediately postmortem, the Femur-MCL-Tibia complexes (FMTCs) were carefully dissected from the hind limbs, wrapped in gauze moistened with phosphate buffered solution, sealed in plastic, and stored frozen (-20^{o}C). Four FMTCs, two from each age group, were damaged during dissection and, hence, were excluded from the study.

Before mechanical testing, the FMTCs were thawed at room temperature. The soft tissues around the knee joints were removed to expose the MCLs (see Figure 3.1(a)) while keeping them hydrated by constantly spraying phosphate buffered saline solution on their surface.

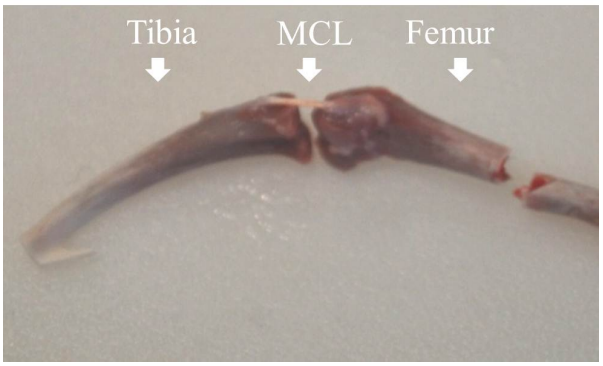

(a) Femur-MCL-Tibia complex (FMTC)

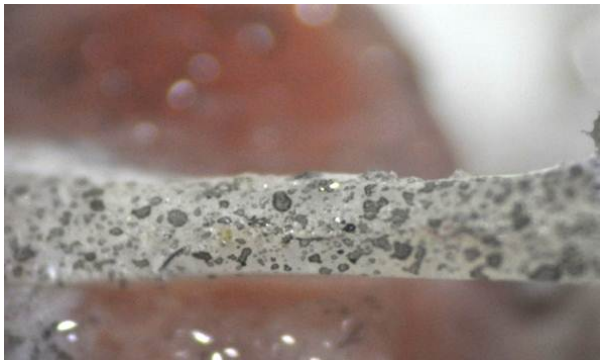

(b) Ink was sprayed on ligament surface

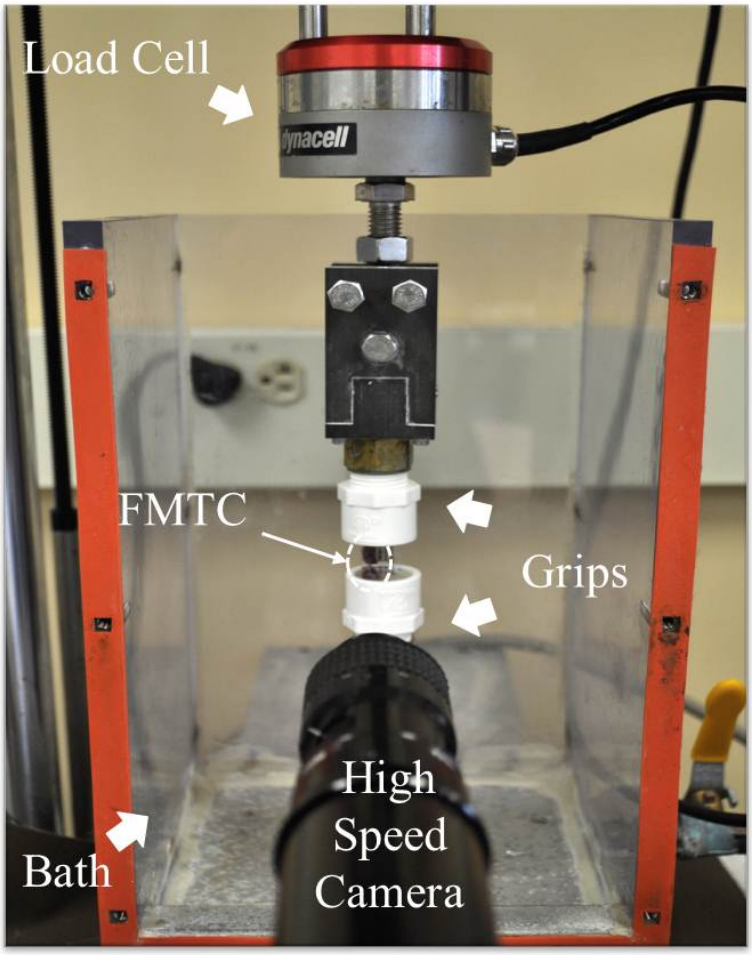

(c) Tensile testing system

Figure 3.1: Experimental Setup

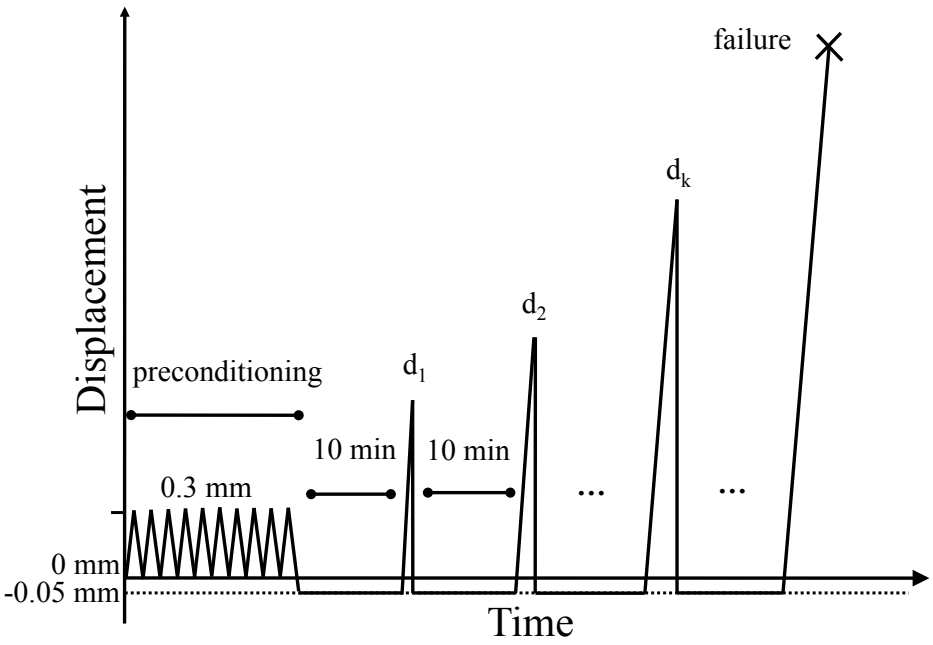

Figure 3.2: Schematic of the experimental protocol.

Black ink was then sprayed on the surface of the MCLs by using an airbrush (Badger Model 150, Franklin Park, IL) to produce markers with suitable contrast for strain calculation (see Figure 3.1(b)). The cross-sectional areas of the MCLs were calculated by assuming elliptical cross-sections. The major and minor axes of the cross-section were measured optically using images taken by a digital camera (Nikon D 5000) under a dissection stereoscope (Zeiss Stemi 2000C). Each measurement was taken three times and averaged.

A strip of fiberglass was attached to the femur of each FMTC using cyanoacrylate glue to reinforce its growth plate while 3 notches ($\sim$ 2mm wide and $\sim$ 2mm deep) were created on the tibia to enhance gripping. The tibia and femur in each FMTC were attached to a frame made of a clear plastic sheet (polyethylene terephthalate copolymer) at a 70-degree flexion

to ensure that the MCL was loaded in its anatomic direction [28, 34]. The bones and plastic frame were potted with bone cement in two hose barbs.

The hose barbs were secured to the mechanical grips of a universal tensile testing machine (Instron ElectroPuls E1000) with vertical mounting. The load cell used had a capacity of 250 N and resolution of 0.001 N. The tibial end of the FMTCs was attached to the upper grip connected to the load cell and the femoral end to the lower grip fixed to a supporting table. Special care was taken to ensure that the FMTCs were aligned along the axis of the load cell. The plastic frames holding the bones were then cut and the FTMCs and grips were immersed in a custom designed bath filled with phosphate buffered saline solution. The experimental setup is shown in Figure 3.1(c).

During testing, the load data were recorded by the load cell of the tensile testing machine. For each MCL the nominal stress data were calculated by dividing the load data by its initial cross-sectional area. The displacement of three black ink markers on the surface of the MCLs was tracked by a video camera (Photron Ultima APX-RS) at a resolution of 256×1024. It was measured in pixels by using imaging analysis software (ProAnalyst, Xcitex). The Green-Lagrangian strain data in the direction of loading were then computed from the displacement data by assuming that the MCLs underwent uniform extension. The visual noise was measured to be approximately 0.07% at 0N load using outlier detection method with 1.5 interquartile range.

Displacement controlled tensile tests were performed on the sixty MCLs isolated from the two age group of rats. The experimental protocol is schematically presented in Figure 3.2. Firstly,

the MCL was preconditioned with 10 stretching cycles up to 0.3 mm at 1 Hz, unloaded to -0.05 mm displacement to assure that the initial state was at 0 N load, and allowed to recover for 10 minutes [1]. After preconditioning and starting from a 0 N load state, the MCL was stretched to a set of incremental displacements, d_k ($k = 1, 2, 3, \ldots$) with $d_{k+1} - d_k = 0.2$ mm, at a displacement rate of 0.1 mm/s until failure occurred. Between consecutive stretches at incremental displacements the MCL was unloaded and allowed to recover for 10 minutes.

3.3 Results

The typical axial stress-strain data collected when testing one of the sixty FMTCs are shown in Figure 3.3. Each stress-strain curve reported in Figure 3.3 was obtained by stretching one FMTC to a single displacement d_k and using the 0 N load as the reference configuration. It can be clearly seen that, as the displacement d_k increased, the elongation of the toe region of the stress-strain curve increased while the tangent modulus of the linear region decreased. These changes in the tensile response of the MCL after consecutive stretching up to different and increasing displacements d_k indicated the initiation and propagation of damage.

The elongation of the toe region of the stress-strain curve determined by stretching the FMTC up to the displacement d_k was quantified by measuring the difference, $\Delta\varepsilon_{0.1}^{(k)}$, between the strain corresponding to the displacement d_k at 0.1 N load, $\varepsilon_{0.1}^{(k)}$, and the strain corresponding to the displacement $d_1 = 0.45$ mm at 0.1 N, $\varepsilon_{0.1}^{(1)}$. Due to noise in the strain measurement, only $\Delta\varepsilon_{0.1}^{(k)} > 0.1\%$ was assumed to indicate the elongation of the toe region. For example,

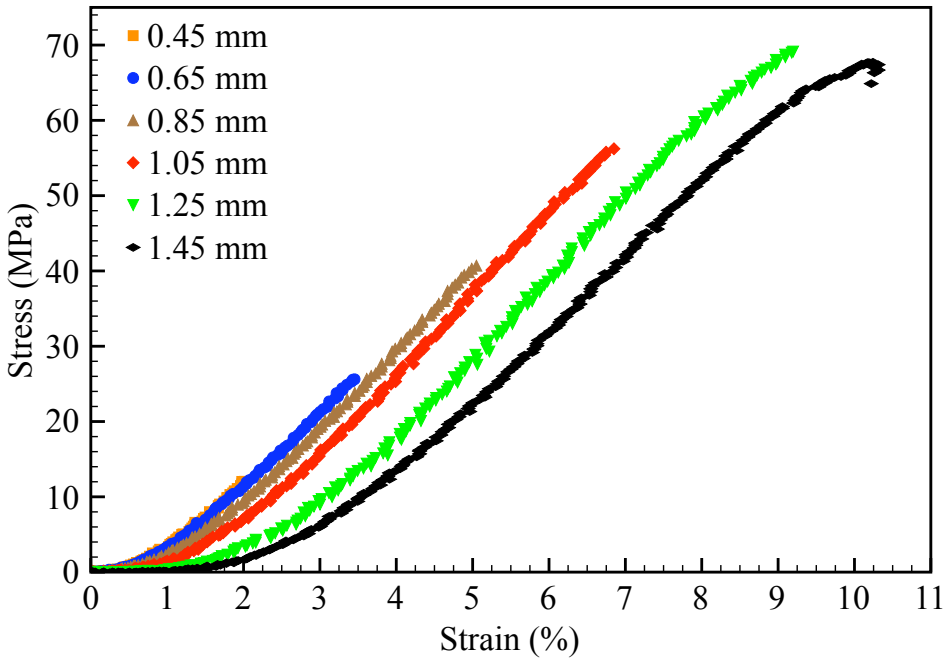

Figure 3.3: Typical tensile axial stress-strain data computed by loading one FMTC to consecutive and increasing displacements as reported in the legend ($d_1 = 0.45$ mm, $d_2 = 0.65$ mm, $d_3 = 0.85$ mm, $d_4 = 1.05$ mm, $d_5 = 1.25$ mm, $d_6 = 1.45$ mm).

for the stress-strain data presented in Figure 3.3, $\Delta\varepsilon_{0.1}^{(k)}$ are computed as demonstrated in Figure 3.4. It can be observed that the first two consecutive displacement d_1 and d_2 did not produce a significant elongation of the toe region. The third displacement d_3 produced an elongation of the toe region, which is manifested when stretching the FMTC to the fifth displacement d_4.

The 0.1 N load was chosen as the preload value in order to eliminate the slack in the MCLs and standardize their initial configuration. The strain was then recalculated with respect to this initial configuration. The stress-strain data in Figure 3.3 are presented with a 0.1

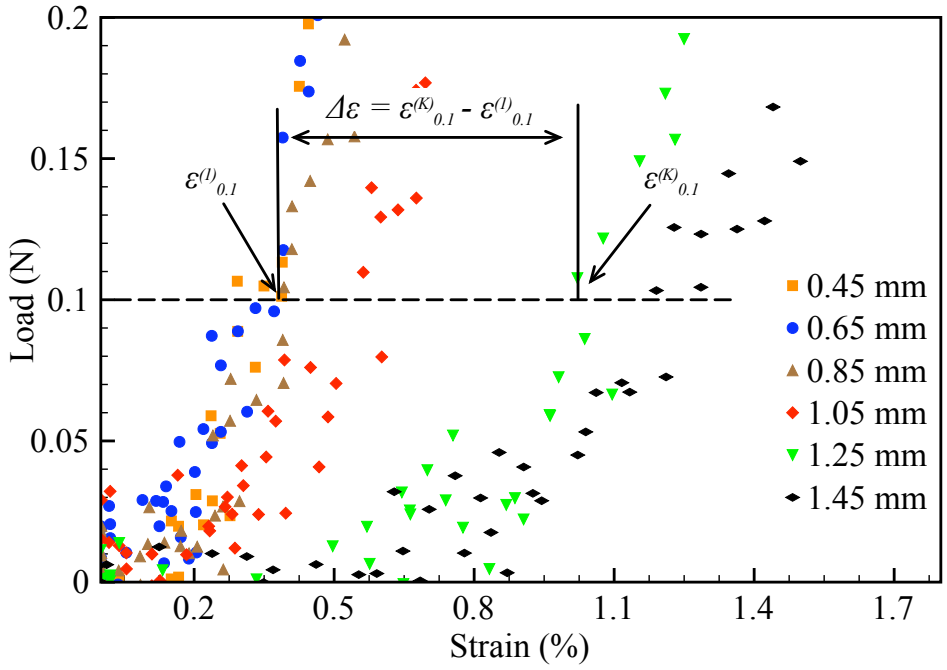

Figure 3.4: Elongation of the toe region for the stress-strain data presented in Figure 3.3. The elongation of the toe region is measured by $\Delta\varepsilon_{0.1}^{(k)}$, which is defined as the difference between the strain corresponding to the displacement d_k at 0.1 N load, $\varepsilon_{0.1}^{(k)}$, and the strain corresponding to the displacement $d_1 = 0.45$ mm at 0.1 N, $\varepsilon_{0.1}^{(1)}$. Note that $k = 6$ for the $\Delta\varepsilon_{0.1}^{(k)}$ shown here.

N preload in Figure 3.5. The strain corresponding to the maximum load associated with each displacement d_k, $\varepsilon_{max}^{(k)}$, and the tangent modulus of the linear region of the stress-strain curve, $E(k)$, were computed.

The elongation of the toe region of the stress-strain curve measured by $\Delta\varepsilon_{0.1}^{(k)}$ and the decrease in the tangent modulus $E(k)$ of the linear region observed when stretching the FMTC up to the displacement d_k were considered to be determined by damage that occurred during the

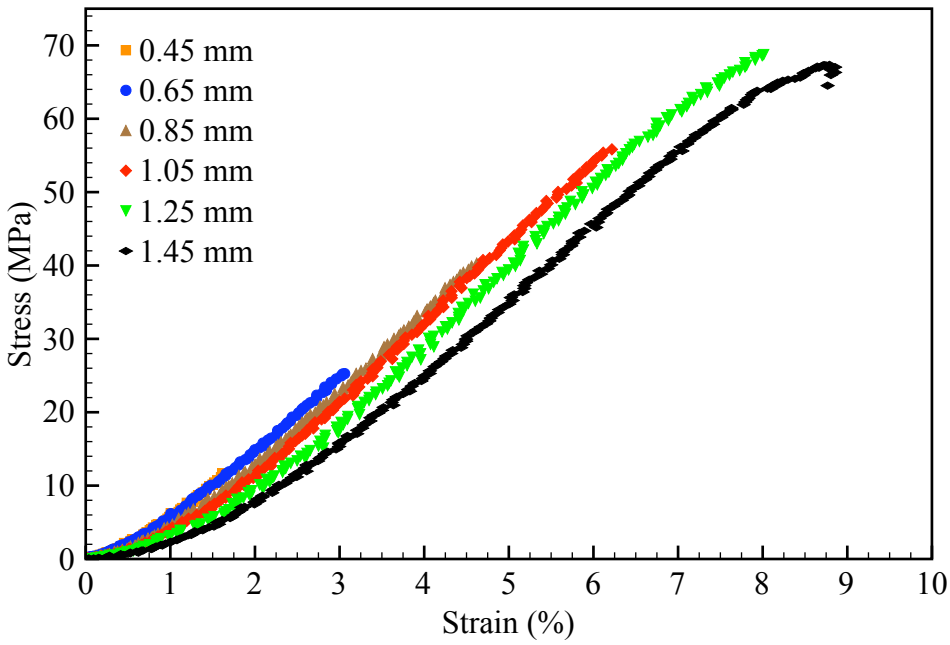

Figure 3.5: Stress-strain data in Figure 3.3 re-plotted by considering a 0.1 N preload.

previous stretching up to the displacement d_{k-1} and, thus, were associated with the corresponding strain $\varepsilon_{max}^{(k-1)}$. In Figure 3.6, both $\Delta\varepsilon_{0.1}^{(k)}$ and $E(k)$ computed from the stress-strain data presented in Figures 3.3, 3.4, and 3.5 are plotted versus the strain $\varepsilon_{max}^{(k-1)}$ for $k = 1, \ldots, 6$ where $\varepsilon_{max}^{(0)} = 0$. The results presented in Figure 3.6 indicate that the elongation of the toe region and the decrease in the tangent modulus occurred at two very different threshold strains denoted with a red-filled circle and a blue-filled square, respectively. Specifically, the elongation of the toe region began at a smaller strain than the decrease in tangent modulus of the linear region. $\Delta\varepsilon_{0.1}^{(k)}$ started to increase at 4.62% threshold strain and $E(k)$ started to decrease at 6.22% threshold strain.

The axial stress-strain data collected from the sixty FMTCs, thirty from each age group,

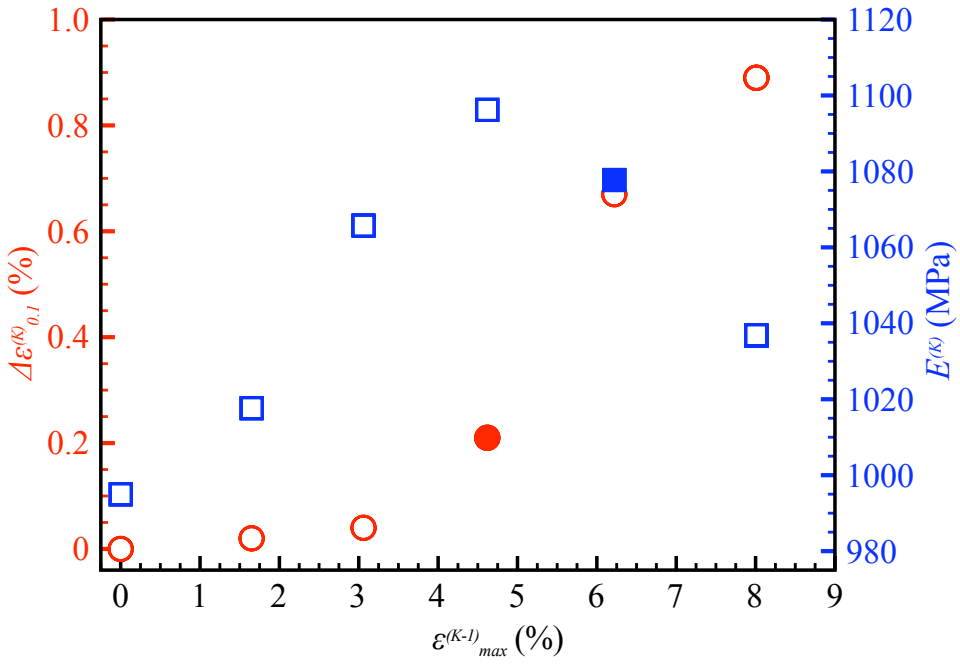

Figure 3.6: Elongation of the toe region, $\Delta\varepsilon_{0.1}^{(k)}$, and tangent modulus of the linear region, $E^{(k)}$, versus $\varepsilon_{max}^{(k-1)}$. Recall that $\varepsilon_{max}^{(k-1)}$ determined the damage quantified by $\Delta\varepsilon_{0.1}^{(k)}$ and $E^{(k)}$ $(k = 1, \ldots, 6)$. Note that $\varepsilon_{max}^{(0)} = 0$ by definition.

were analyzed for damage. The threshold strains associated with the elongation of the toe region and decrease in the tangent modulus of the linear region were computed. For the FMTCs isolated from the younger rats, the strain thresholds are shown in Figure 3.7 in a box plot. The strain associated with the elongation of the toe region was found to be 2.61±1.33% while the strain associated with the decrease in tangent modulus of the linear region was determined to be 4.87±1.99%. For the thirty FMTCs isolated from the older rats, these two threshold strains were 2.84±1.29% and 5.51±2.10%, respectively. The results for this second group of rats are shown in Figure 3.8 in a box plot. Again, one can observe

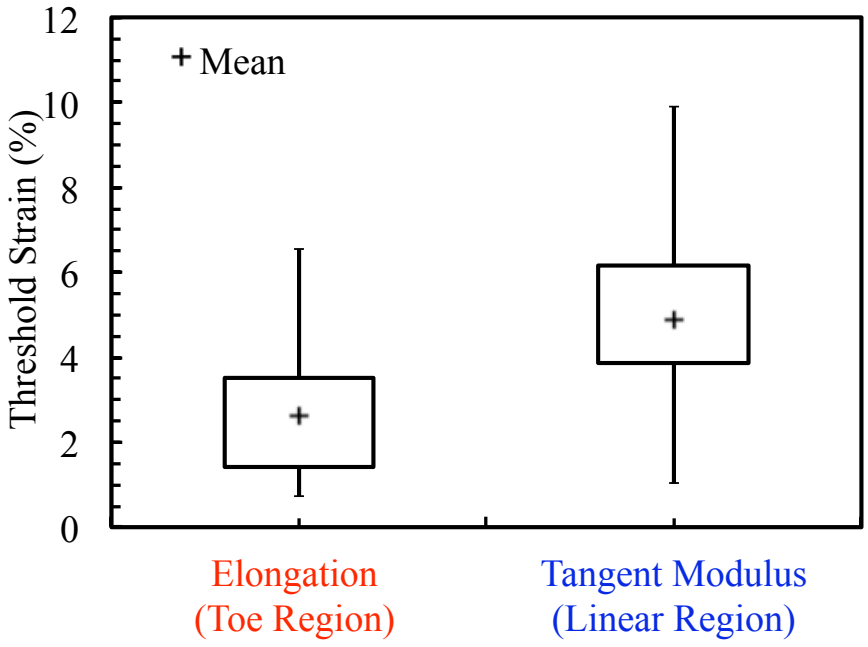

Figure 3.7: Damage strain thresholds for $n = 30$ MCLs (57±1 days old rats).

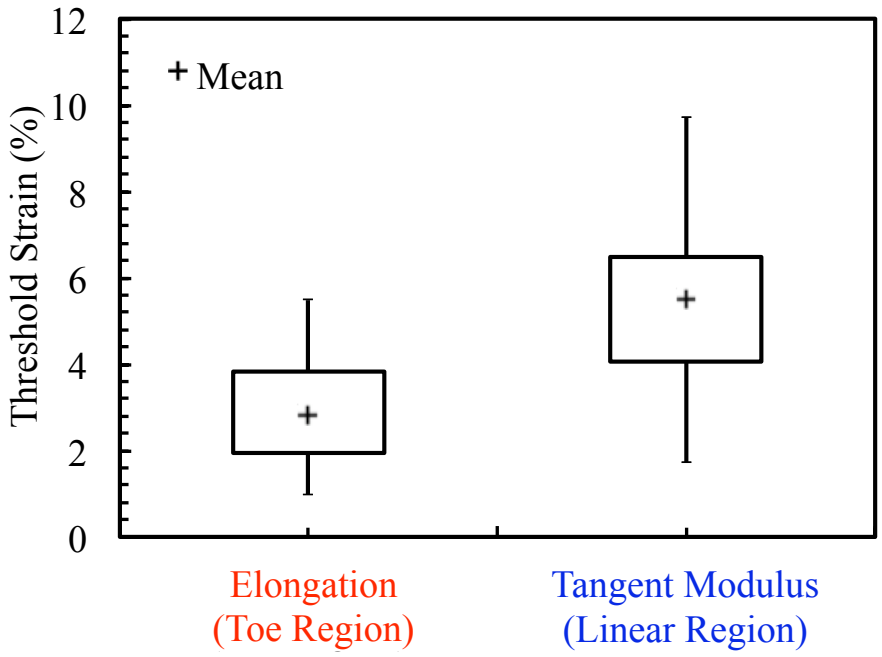

Figure 3.8: Damage strain thresholds of $n = 30$ MCLs (84±3 days old rats).

that the elongation of the toe region occurred at lower threshold strain than the decrease in tangent modulus of the linear region.

Most of specimens failed at the tibia insertion site. Only 2 MCLs from the younger rat group and 6 MCLs from the older rat group failed at the ligament's midsubstance.

Statistical analysis of the experimental data was done through Wilcoxon test by JMP software (JMP, Version 9.0, SAS Institute Inc., Cary, NC, 1989-2010). The p-value, which is called the observed significance level, was computed to determine the difference between the two damage phenomena in each age group and the difference between the damage phenomena between the two age groups. Specifically, to compare the difference between the means of

two groups of experimental data, a null hypothesis was made according to which the means of the two groups of experimental data were the same. The smaller the p-value, the stronger the observed result against the null hypothesis is. If the p-value is less than a threshold value, the null hypothesis is rejected and the means of two groups of experimental data can be said to be significantly different. In this study the statistical significance was established at $p<0.05$, which is a value commonly used in statistics [101].

For both age groups, statistical analysis showed that there was a significant difference between the threshold strains indicating the elongation of the toe region and the decrease in tangent modulus of the linear region of the axial stress-strain curve of MCLs ($p<0.05$). Although these two threshold strains were higher ($2.84\pm1.29\%$ compared to $2.61\pm1.33\%$, and $5.51\pm2.10\%$ compared to $4.87\pm1.99\%$) for MCLs isolated from older rats than for MCLs isolated from younger rats, the differences were not statistically significant ($p>0.05$).

3.4 Discussion

In this study, mechanical damage in ligaments was investigated by performing displacement-controlled tensile tests on MCLs excised from two age groups of rats. The MCLs were stretched multiple times to different and increasing displacements until its failure occurred. Two different phenomena, which indicated the initiation of damage, were observed from the collected tensile axial stress-strain curves: the elongation of the toe region and decrease in tangent modulus of the linear region. The strains that produced these changes in the

stress-strain curves were computed and found to be significantly different.

Previous studies on fatigue and cyclic tests on parallel-fibered collagenous tissues suggested that the elongation of the toe region [51, 98, 99] and decrease in tangent modulus (or stiffness) [52, 96, 97] of the linear region of the stress-strain (or load-deformation) curve are indicators of tissues' damage. Experiments conducted by stretching these tissues monotonically also produced similar results [31].

More recently, Provenzano et al. [1] conducted tensile tests on rat MCLs in order to determine the onset of structural damage. In their experimental protocol, each specimen was subjected to a single stretch, unloaded, allowed to recover from creep, and then stretched to failure. Structural damage was defined by the authors as the change in ligament length measured at 0.1 N preload produced by a single stretch. The authors estimated that structural damage initiates at 5.14% strain. In our study, the increase in the elongation of the toe region at 0.1 N preload, which is associated with an increase in ligament length, was found to occur at much lower strains: $2.61 \pm 1.33\%$ for younger rats and $2.84 \pm 1.29\%$ for older rats. Moreover, while in the study by Provenzano et al. [1] the decrease in tangent modulus of the linear region was reported with the increase in ligament length, in our study it was found to occur at significantly different strains: $4.87 \pm 1.99\%$ for younger rats and $5.51 \pm 2.10\%$ for older rats. These differences are, most probably, due to different experimental protocols and methods used to determine the onset of structural damage. According to Panjabi et al. [100], single and incremental subfailure stretches are mechanically equivalent in producing damage. Thus, the protocol used in our study is similar to the one used in [1] but provides more accurate

determination of the threshold strain for each tested rat MCL.

In the experimental protocol used in this study, the threshold strains were computed by analyzing the increase in elongation of the toe region and the decrease in the tangent modulus of the linear region of the stress-strain curve that occurred after loading the MCLs to consecutive displacements, d_k with $k = 1, 2, \ldots$, which were incrementally increased by 0.2 mm, i.e. $d_{k+1} - d_k = 0.2$ mm. Clearly, the values of the computed threshold strains are strongly dependent on the displacement increment of the experimental protocol and are likely overestimated. For example, for the representative data reported in Figure 3.6, the increase in elongation of the toe region and the decrease in tangent modulus of the linear region of the stress-strain curves were caused by $\varepsilon^{(3)}_{max}$=4.62% (or $d_3 = 0.85$ mm) and $\varepsilon^{(4)}_{max}$=6.22% (or $d_4 = 1.05$ mm), respectively. However, it is possible that the increase in elongation of the toe region started at a strain larger than $\varepsilon^{(2)}_{max}$=3.06% and smaller than $\varepsilon^{(3)}_{max}$=4.62% or, equivalently, at a displacement larger than $d_2 = 0.65$ mm and smaller than $d_3 = 0.85$ mm. Similarly, the decreased in tangent modulus was observed to occurr at a strain larger than $\varepsilon^{(3)}_{max}$=4.62% and smaller than $\varepsilon^{(4)}_{max}$=6.22% or, equivalently, at a displacement larger than $d_3 = 0.85$ mm and smaller than $d_4 = 1.05$ mm. Clearly, by using smaller displacement increments in the experimental protocol, a more accurate measurement of the damage threshold strains can be achieved.

It is speculated that the two different damage phenomena, the elongation of the toe region and the decrease in tangent modulus of the linear region of the tensile axial stress-strain curve, are determined by different micro-structural variations induced by strain in the liga-

mentous tissue. The tensile response of ligaments in the toe region is believed to be caused mainly by the un-crimping of the collagen fibrils and/or fibers [102]. Thus, it is possible that the elongation of the toe region is caused by an increased initial waviness of the collagen fibrils and/or fibers that result from alterations in the fiber-fiber and fiber-matrix interactions. The decrease in tangent modulus of the linear region is, most probably, caused by the breakage of collagen fibrils/fibers in the tissue. Future studies will be conducted to reveal the micro-structural origin of damage in the MCLs.

In our experiments, failure of the FMTCs upon stretching occurred mostly at the tibial insertion site (28/30 for younger rats and 24/30 for older rats). The finding is consistent with recent studies on the effect of cyclic stretching on FMTCs isolated from older Sprague-Dawley rats [29]. The failure near or at the insertion site was likely determined by the morphology of the FMTCs. In Sprague-Dawley rats with age up to 120 days, the MCL inserts into the tibia only through the periosteum with no fibrocartilage zone [103]. Due to the absence of the fibrocartilage zone, the tibial insertion site was strained more and, consequently, failed more often during tensile testing. In addition, the strain near or at the tibial insertion site was found to be higher than the strain near or at the femoral insertion site also in canine, swine, and rabbit MCLs [104].

Chapter 4

Microscopic Study of Damage in Ligaments

4.1 Introduction

Sprains are among the most common injuries encountered in sports [4, 8, 11]. First- and second-degree sprains, which consist of subfailure damage to ligaments, are the most frequent [16]. Experimental studies on effect of the subfailure damage on the mechanical properties of ligaments have been conducted by several researchers [1, 27, 31, 50–53]. In these studies, monotonic loading [1, 27, 31] and cyclic loading [50–53] were applied to different types of ligaments. The damage was observed as decrease in peak load during cyclic loading [50, 51], decrease in tangent modulus/stiffness [1, 27, 31, 52, 53] and elongation of the toe

region [1, 27, 31, 50–52]. In our study (see Chapter 3), rat MCLs were loaded to consecutive and increasing stretches and the changes in the recorded tensile axial stress-strain curves were analyzed. Non-recoverable elongation of toe region and decrease in tangent modulus of the linear region were observed in MCLs harvested from two age groups of rats. Statistical analysis demonstrated that these two damage phenomena occurred at two significantly different strains.

Little is known about the mechanisms of damage in ligaments. Clearly, the damage in ligaments is determined by the damage of their structural components. Provenzano et al. [1] suggested that the torn or plastically deformed collagen fibers and the biochemical degradation of the extracellular matrix may be responsible for the increased toe region observed in their experiments. Thornton et al. [52] speculated that the reduced tangent modulus measured in upper 50% of the cyclic loading curve and increased toe region were due to the rupture of collagen fibers and damage occurring in the extracellular matrix. It is well known that the collagen fibers and fibrils are the major tensile load carriers in ligaments [105]. Thus, changes in the morphology of collagen fibers and fibrils may determine the different mechanical behavior of damaged ligaments.

Scanning Electron Microscopy (SEM) has been used to investigate the internal microstructure of ligaments. Frank et al. [106] studied the alignment of collagen fibers in scar tissues of healing ligaments. Hurschler et al. [107] used SEM to compare the difference in the morphology of collagen fibers in normal and healing rat MCLs. The SEM technique has also been employed to characterize the collagen fibrils' morphology and organization in different

animals [108]. Moreover, the typical crimp of collagen fibrils in ligaments and tendons has been investigated using SEM by several investigators [109–111]. The successful use of SEM in these studies proved that this technique is capable of providing important information on the morphology of collagen fibers and fibrils.

A few studies investigated microscopic damage at the collagen fiber- and fibril-levels that occur during mechanical loading. Microscopic damage to collagen fibers and fibrils in ligaments subjected to different strains were examined using SEM in [112] and [113]. Yahia et al. [112] examined rabbit MCLs, which were previously stretched to different strain levels, under SEM. They reported different levels of collagen fiber ruptures at 10% and 20% strains. Provenzano et al. [113] observed broken collagen fibrils in SEM images of the rat MCL, which was stretched to 5.8% strain. In these two studies, the microscopic damage were not correlated to the macroscopic mechanical damage. Dodds et al. [114] used light microscopy to examine the rabbit ACL stretched to a subfailure deformation defined as 75% of the failure deformation. The collagen fibers appeared more distorted after subfailure deformation but no information about the collagen fibrils was provided in their study.

In this chapter, the role of collagen fibers and fibrils in determining the mechanical damage (elongation of toe region and decrease in tangent modulus of the linear region of the tensile axial stress-strain curve) described in Chapter 3 will be studied using SEM. Toward this end, rat MCLs will be stretched to different values of the tissue's displacement and their mechanical damage will be analyzed using the same methods described in Chapter 3. The ligaments will be then prepared and examined using SEM to investigate the micro-structural

changes associated with the observed strain-induced damage phenomena.

4.2 Materials and Methods

4.2.1 Materials

This study was conducted in accordance with applicable laws, regulations, guidelines, and policies (i.e., the U.S. Animal Welfare Act, Public Health Service Policy, U.S. Government Principles, and the Guide for the Care and Use of Laboratory Animals). All procedures were conducted with approval of the Institutional Animal Care and Use Committee at Virginia Tech. Four Sprague Dawley male rats (331.9±3.9 g, body mass) were purchased from Harlan Laboratories (Frederick, MD). The rats were euthanatized with 4 ml of Beuthanasia D solution intraperitoneal injection (phenytoin and pentobarbital; each ml: active ingredients: 390 mg pentobarbital sodium, 50 mg phenytoin sodium). Immediately postmortem, the Femur-MCL-Tibia complexes (FMTCs) were carefully harvested from the hind limbs, wrapped in gauze moistened with phosphate buffered solution, sealed in plastic, and stored frozen (-20^{o}C).

The eight FMTCs were divided into 5 groups based on the level of mechanical stretches they received: slack group (n=1, specimen s_1 from rat 1), preconditioned and unloaded group (n=2, specimens p_1 from rat 1 and p_2 from rat 2), undamaged group (n=2, specimens u_1 from rat 2 and u_2 from rat 3), low damaged group (n=2, specimens ld_1 from rat 3 and ld_2

from rat 4) and high damaged group (n=1, specimen hd_1 from rat 4).

4.2.2 Protocol for Mechanical Experiments

Except for the MCL in the slack group, the remaining seven MCLs were prepared for mechanical testing and tested using the methods described in Chapter 3. The experimental protocols used for the FMTCs in the preconditioned and unloaded group (n=2), undamaged group (n=2), low damaged group (n=2), high damaged group (n=1) were different. Under displacement control, the FMTCs from each group were preconditioned (stretched to 0.3 mm for 10 cycles at 1Hz) and maintained at 0 N load state for 10 minutes to allow recovery from viscoelastic effects. After preconditioning and 10 minutes recovery, the FMTCs in the preconditioned and unloaded group were kept at the 0 N load state and fixed for SEM analysis as described in detail later. The FMTCs in undamaged, low damaged, and high damaged groups were stretched using a 0.1mm/s displacement rate up to the displacements $d_u = 0.45$ mm, $d_{ld} = 0.95$ mm, and $d_{hd} = 1.45$ mm, respectively. These values of the displacements were chosen since, in our previous study presented in Chapter 3, we found that an average displacement of 0.45 mm did not produce mechanical damage, an average displacement of 0.95 mm produced an elongation of the toe region and could cause a decrease in tangent modulus of the linear region, an average displacement of 1.45 mm produced a decrease in tangent modulus of the linear region and elongation of the toe region. The load was removed immediately after the target displacements were achieved and the MCLs were allowed to recover for 10 minutes. They were then stretched again to the same displacements used during

the first stretching and held at these displacements for SEM fixation.

4.2.3 Analysis of Mechanical Data

Tensile axial stress-strain data were computed from load-deformation data for the MCLs in the undamaged, low damaged, and high damaged groups in order to determine the level of mechanical damage. By using methods similar to those described in Chapter 3, the elongation of the toe region and decrease in tangent modulus of the linear region of the stress-strain curve observed after the second stretching were quantified. The elongation of the toe region of the stress-strain curve was defined as $\Delta\varepsilon_{0.1}^{(2)} = \varepsilon_{0.1}^{(2)} - \varepsilon_{0.1}^{(1)}$, where $\varepsilon_{0.1}^{(2)}$ is the strain computed during the second stretching at 0.1 N load and $\varepsilon_{0.1}^{(1)}$ is the strain computed during the first stretching at 0.1 N load. The strains, $\varepsilon_{0.1}^{(1)}$ and $\varepsilon_{0.1}^{(2)}$ were computed by assuming the 0 N load as the reference configuration. The 0.1 N load was then chosen as the preload value in order to eliminate the slack in the MCLs and standardize their initial configuration. The strain corresponding to the maximum load associated with the displacement $d_u = 0.45$ mm, $d_{ld} = 0.95$ mm, or $d_{hd} = 1.45$ mm was then calculated by assuming that the 0.1 N load configuration was the reference configuration.

4.2.4 Sample Preparation for SEM

Immediately after mechanical testing, the FMTCs in the preconditioned and unloaded, undamaged, low damaged, high damaged groups were fixed for 1 hour using a fixative, which

consisted of 2.5% glutaraldehyde in 0.1 M sodium cacodylate buffer (Electron Microscopy Science, Hatfield, PA). The fixative was sprayed constantly for 1 hour on strips of paper towel, which were wrapped around the surface of the MCLs, while the FMTCs were kept mounted on the tensile testing machine. The MCLs were then carefully isolated from the femurs and tibias and stored in the fixative for at least 24 hours. The MCL in slack group, which was not mechanically tested, was also carefully isolated from the femur and tibia and placed into the fixative for at least 24 hours. After fixation, the MCLs were placed under a dissection stereoscope (Zeiss Stemi 2000C) and fractured along the sagittal plane (Figure 4.1) with a surgical scalpel.

The fractured specimens were sent to the Morphology Service Lab located in the Virginia-Maryland Regional College of Veterinary Medicine for SEM preparation. They were placed in 1% tannic acid for 2 hours, rinsed with cacodylate buffer and post-fixed with 1% O_sO_4 in 0.1 M Na cacodylate buffer for 1 hour. After post-fixing, the MCLs were dehydrated in a graded series of ethanol (15%, 30%, 50%, 70%, 95% and 100% ethanol for 15 minutes each). The MCLs were transferred in a critical point drier for dehydration and then sputter-coated with an approximately 72 nm thick layer of gold. When the above preparation process finished, the specimen was mounted on SEM block for scanning (Phillips 505 Scanning Electron Microscope).

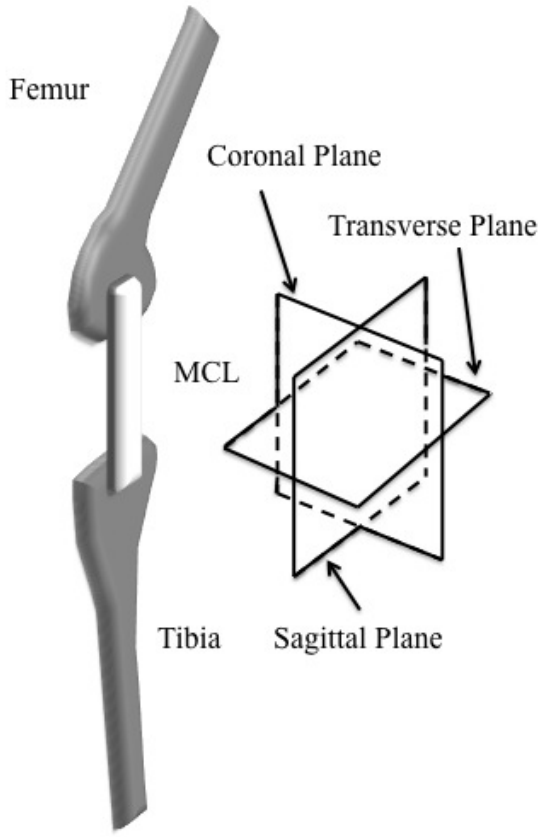

Figure 4.1: FMTC and three imaginary planes of human body

4.3 Results

4.3.1 Mechanical Tests

The elongation of the toe region and the decrease in tangent modulus of the linear region of tensile axial stress-strain curves were computed as previously described for the two MCLs in the undamaged group (u_1 and u_2), the two MCLs in the low damaged group (ld_1 and ld_2), and one MCL in the high damaged group (hd_1).

The MCLs in the undamaged group were stretched to 0.45 mm, unloaded, allowed to recover, and re-stretched up to the same displacement. No significant changes in the toe region and linear region of the stress-strain curves were observed between the first and second stretching to 0.45 mm displacement as shown in Figure 4.2.

The MCLs in the low damaged group were stretched to 0.95 mm, unloaded, allowed to recover, and re-stretched up to the same displacement. This displacement produced an elongation of the toe region of the stress-strain curve that was found to be $\Delta\epsilon_{0.1}^{(2)}$ =0.16% for the specimen ld_1 and $\Delta\epsilon_{0.1}^{(2)} = 0.20\%$ for the specimen ld_2. The tangent modulus of the linear region during the first stretching, $E^{(1)}$, was found to be different than the tangent modulus of the linear region during the second stretching, $E^{(2)}$. Specifically, $E^{(2)} = 85.9\%E^{(1)}$ for the specimen ld_1 and $E^{(2)} = 98.7\%E^{(1)}$ for the specimen ld_2 (Figure 4.3).

The MCL in the high damaged group was stretched to 1.45 mm, unloaded, allowed to recover, and re-stretched to the same displacement. The elongation of the toe region of the stress-

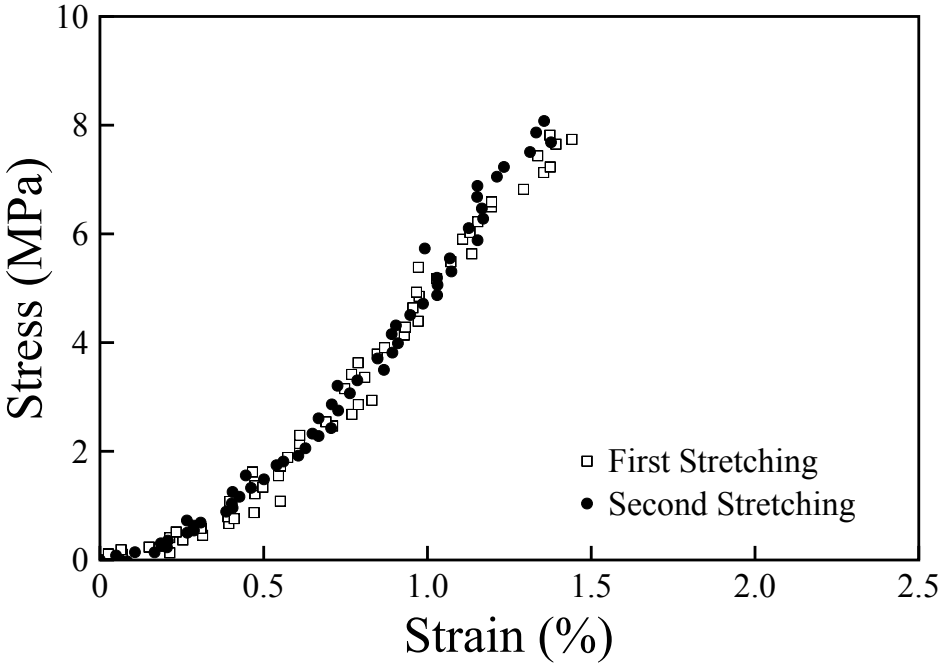

(a) Undamaged group, specimen u_1.

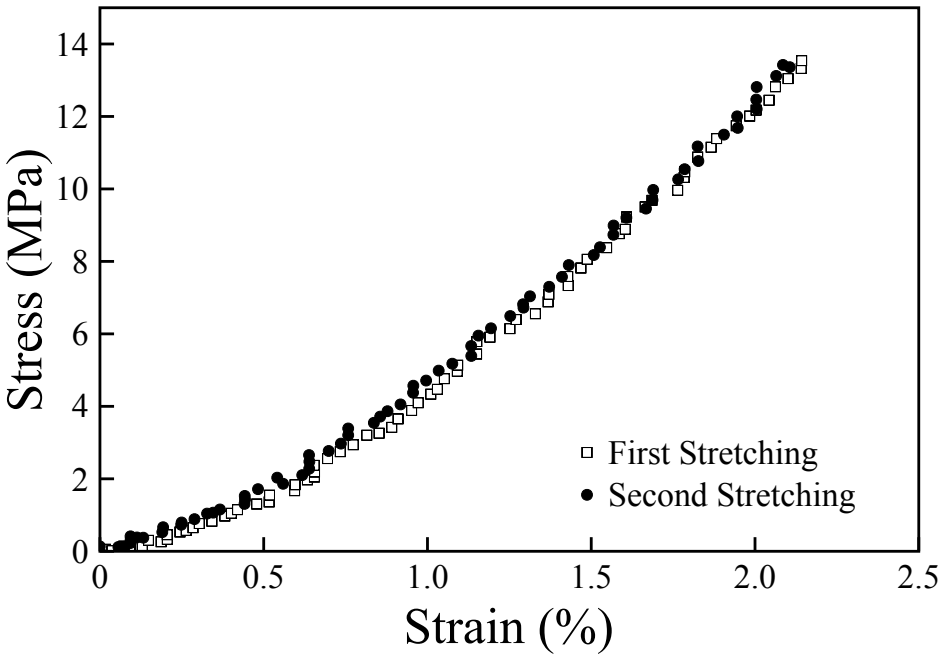

(b) Undamaged group, specimen u_2.

Figure 4.2: Tensile axial stress-strain curves of MCLs stretched to 0.45 mm (undamaged group).

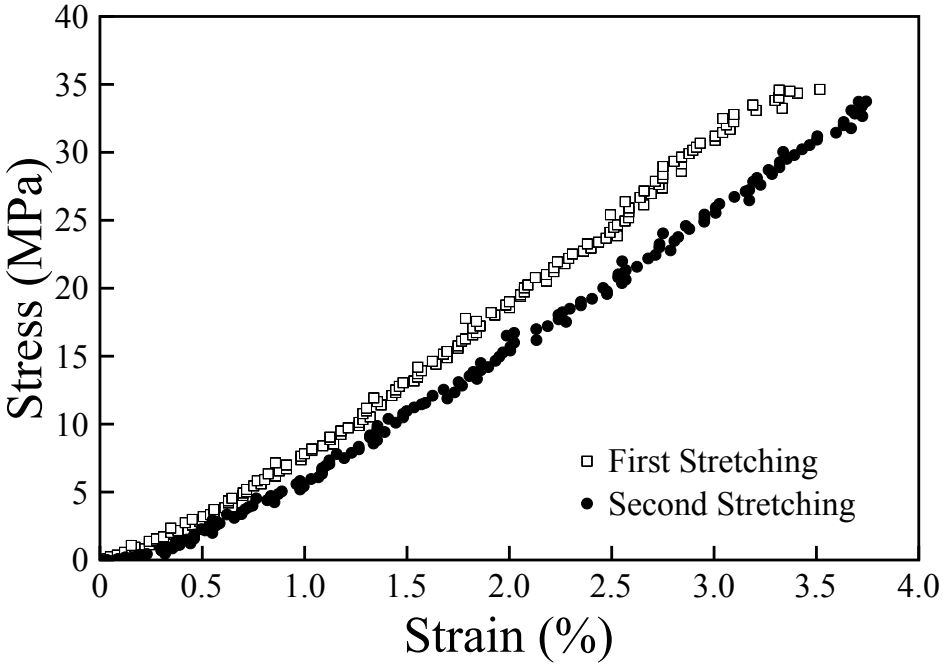

(a) low damaged group, specimen ld_1

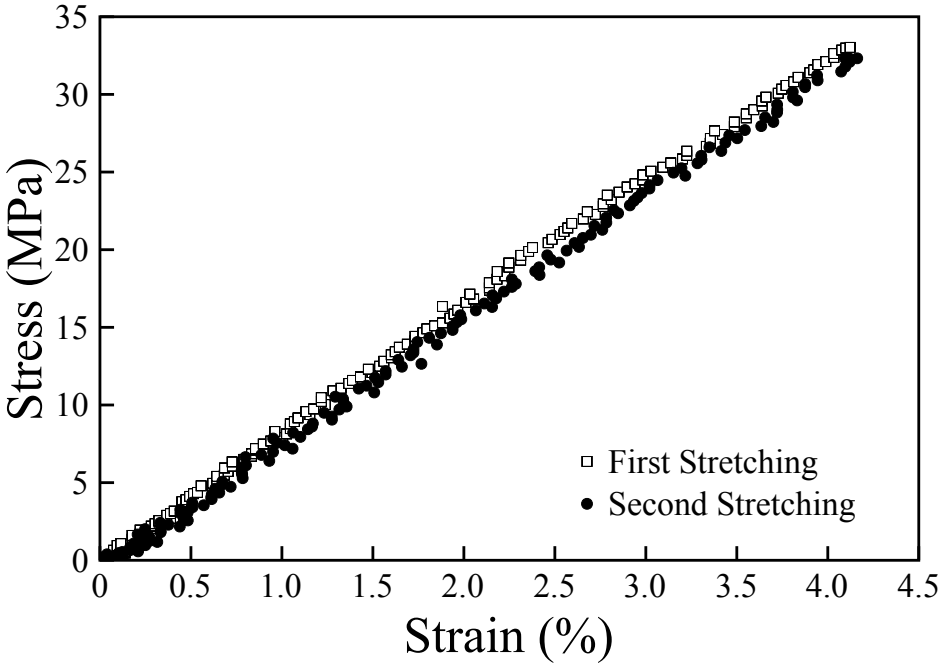

(b) low damaged group, specimen ld_2

Figure 4.3: Tensile axial stress-strain curves of MCLs stretched to 0.95 mm (low damaged group).

strain curve was measured to be $\Delta\epsilon_{0.1}^{(2)}$ =0.69%. The tangent modulus of the linear region recorded during the first stretching decreased during the second stretching: $E^{(2)} = 87.0\%E^{(1)}$ (Figure 4.4).

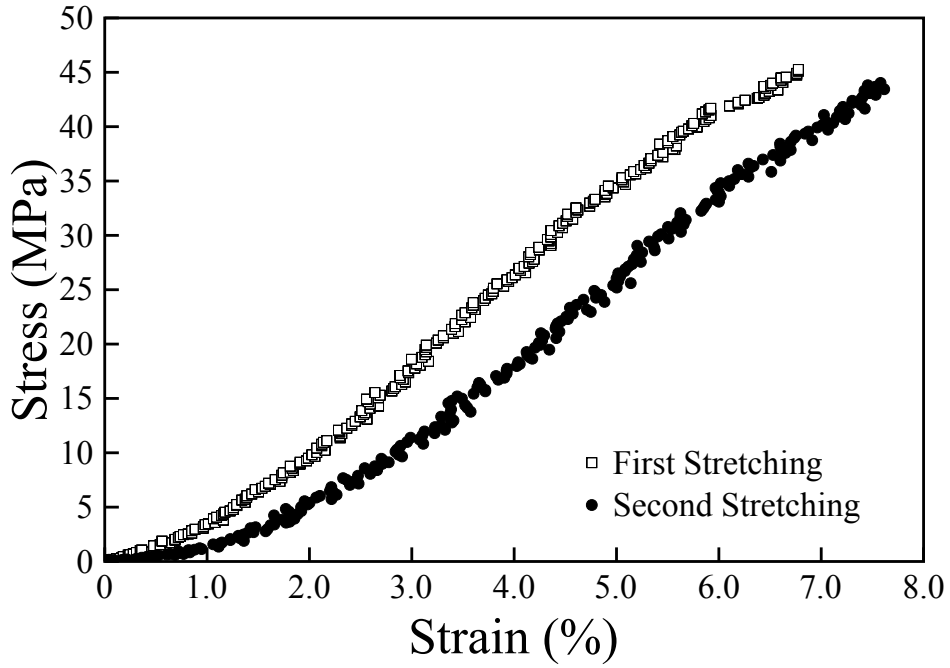

Figure 4.4: Tensile axial stress-strain curve of one MCL (specimen hd_1) stretched to 1.45 mm (high damaged group).

4.3.2 SEM Studies

The sagittal planes of the MCLs from the 5 groups were examined under SEM. For the specimen in the slack group, collagen fibers having different waviness were observed (Figure 4.5(a)). Besides the visible collagen fiber waviness, in some but not all the collagen fibers, the fibrils were also crimped but the crimp patterns were different from the crimp patterns of

the fibers (Figure 4.5(b)). The collagen fibrils exhibited more kinks and larger crimp angles than the collagen fibers.

The two specimens in the preconditioned and unloaded group were not stretched after preconditioning. The collagen fibers appeared to be mainly straight in the specimen p_1 (Figure 4.6(a)) while they presented more waviness in the specimen p_2 (Figure 4.6(c)). Even in this group, in some but not all the collagen fibers, the crimp angles of the fibrils were greater than the crimp angles of the fibers, as shown in Figures 4.6(b) and 4.6(d).

Specimens from the undamaged, low damaged, and high damaged groups were stretched up to different displacements after preconditioning. Most of the collagen fibers in these specimens were found to be straight (Figures 4.7(a), 4.8(a), 4.8(b) and 4.9(a)). The sagittal surface of the specimens was scanned under SEM at low magnification (100X) to find regions of possible damage. These regions were then examined and imaged at high magnification (1000X and 5000X).

The specimens in the undamaged group exhibited less crimped collagen fibrils (Figures 4.7(a) and 4.7(b)) than the specimens in the preconditioned and unloaded group.

Most of the collagen fiber and fibrils of the specimens in the low damaged group were straight (Figures 4.8(a) and 4.8(b)). Regions containing damaged collagen fibers were found in both specimens ld_1 and ld_2 (Figures 4.8(c) and 4.8(d)). In these regions, some of the collagen fibrils in the collagen fibers appeared broken. When comparing specimen ld_1 with specimen ld_2, the regions showing damage were larger and more numerous in the specimen ld_1 than

those in the specimen ld_2 (Figures 4.8(e) and 4.8(f)).

In the specimen of the high damaged group, a large amount of collagen fibers was found to be broken (Figure 4.9(a)). The fractured ends of broken collagen fibers were sharp and clearly visible (Figure 4.9(b)). These characteristics of broken fibers were not observed for the specimens in the low damaged group.

4.4 Discussion

The elongation of the toe region and decrease in tangent modulus of the stress-strain curve during tensile tests up to consecutive and increasing displacements indicate the presence of damage in ligaments. In Chapter 3, these mechanical phenomena were observed to occur at two different threshold strains equal to $2.84 \pm 1.29\%$ and $5.51 \pm 2.10\%$, respectively, for MCLs from SD rats (342.2±15 g, body mass) (see Figure 3.8). In this study, MCLs from SD rats (331.9±3.9 g) were subjected to tensile tests using the experimental methods presented in Chapter 3. The ligaments were, however, stretched only to the critical displacements that were found to produce mechanical damage. In the undamaged group, stretching the specimens u_1 and u_2 to a displacement of 0.45 mm produced strain values of 1.37% and 2.14%, respectively. These strain values are lower than the mean value of the threshold strain at which the toe region in the stress-strain curve elongates (2.84%) and, hence, no significant changes in the stress-strain curve were observed.

The specimens in the low damaged group, ld_1 and ld_2, were stretched to a displacement of

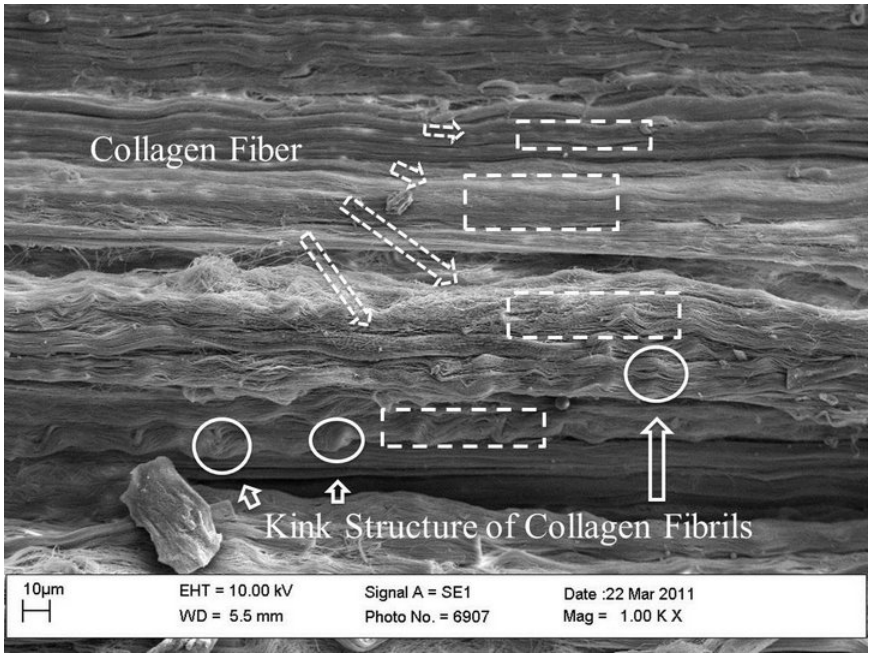

(a) specimen s_1

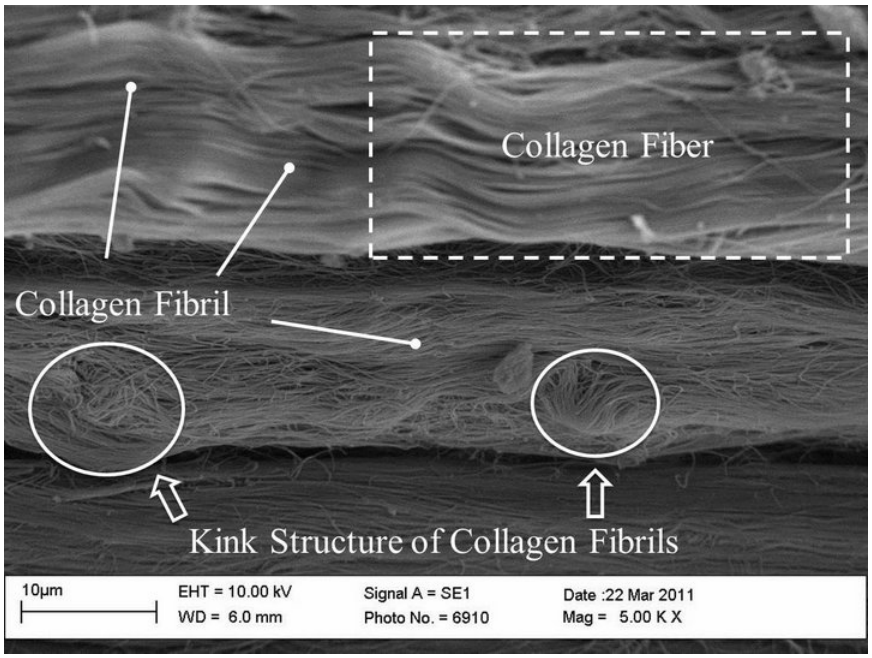

(b) specimen s_1

Figure 4.5: SEM pictures of one MCL not subjected to mechanical testing (slack group).

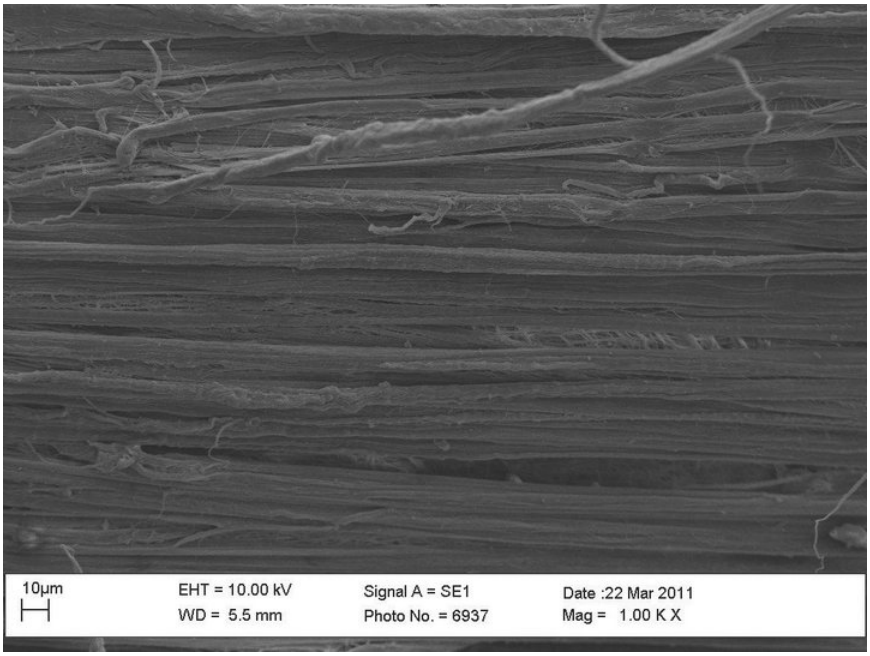

(a) specimen p_1

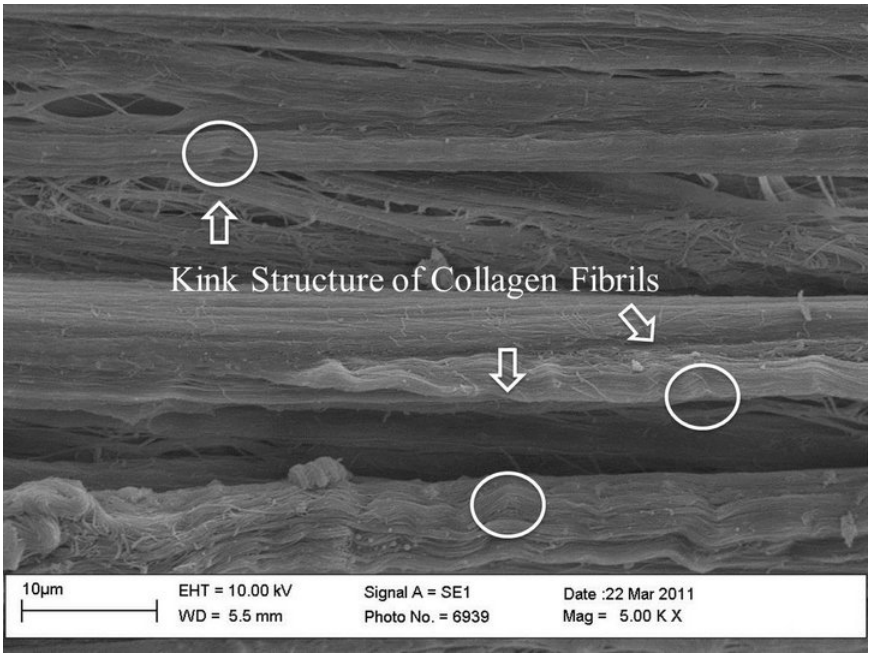

(b) specimen p_1

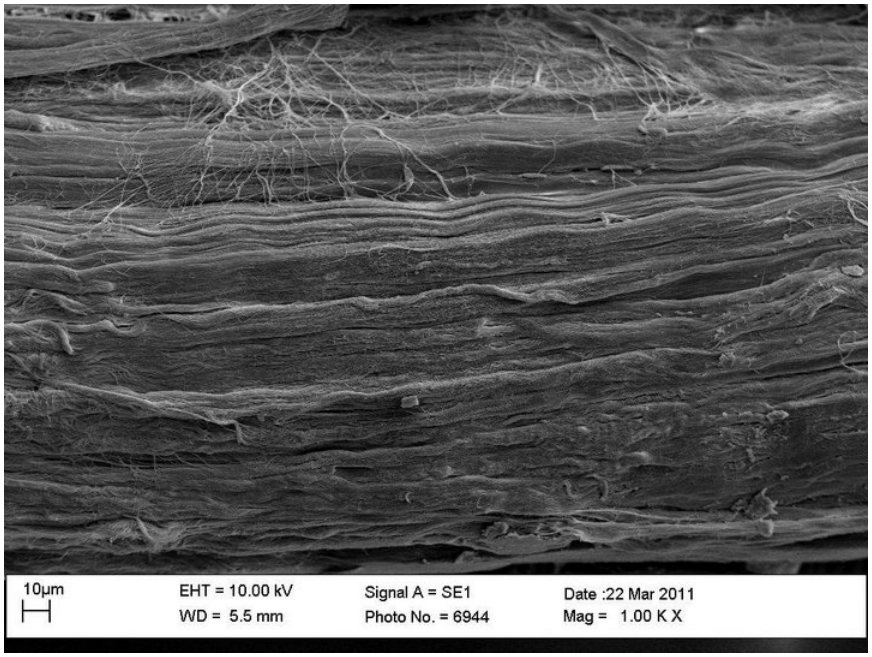

(c) specimen p_2

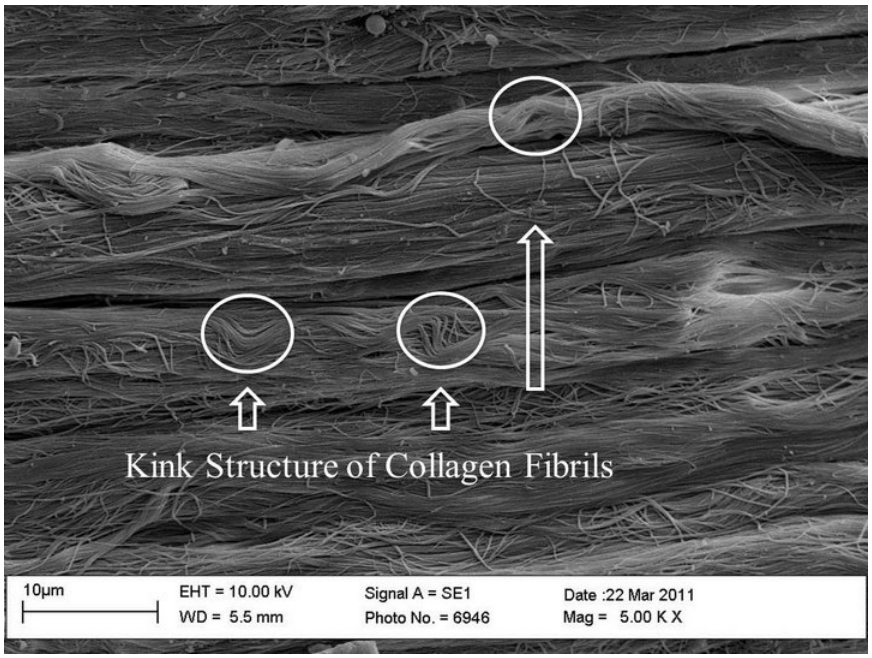

(d) specimen p_2

Figure 4.6: SEM pictures of the two MCLs from the preconditioned and unloaded group at 1000X (a and c) and 5000X (b and d) magnifications.

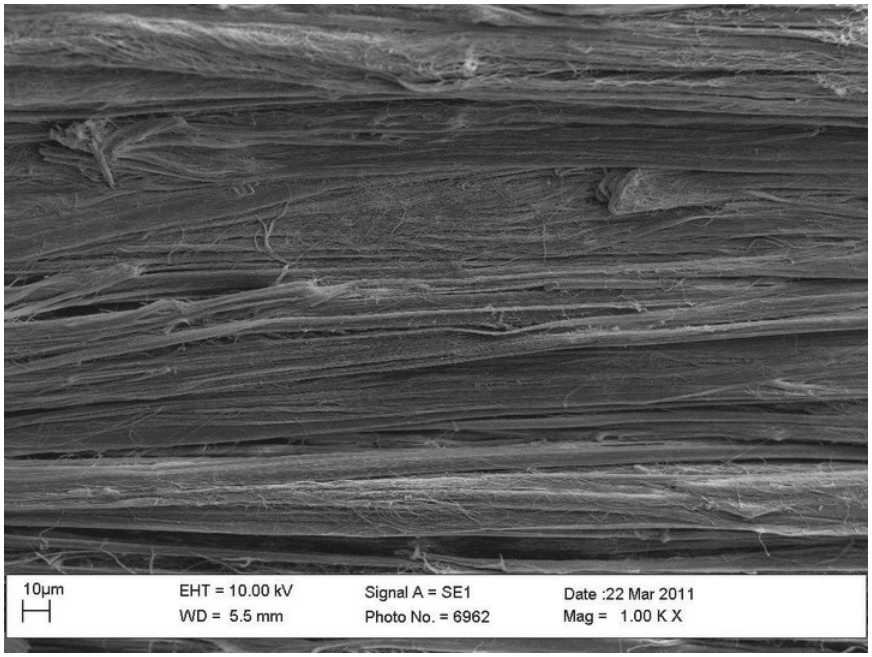

(a) specimen u_1, low magnification

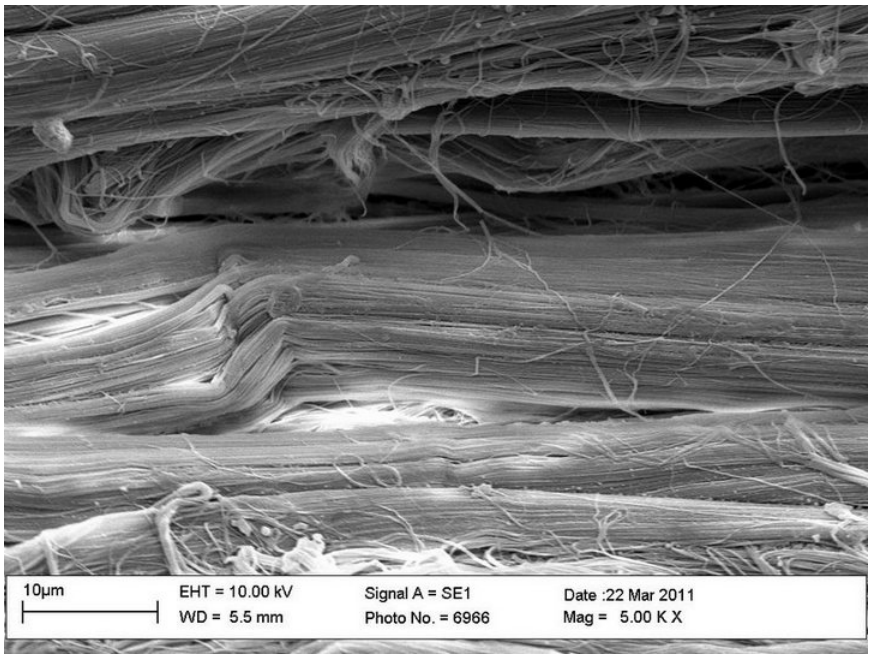

(b) specimen u_1, high magnification

Figure 4.7: SEM pictures of MCLs stretched to 0.45 mm (undamaged group).

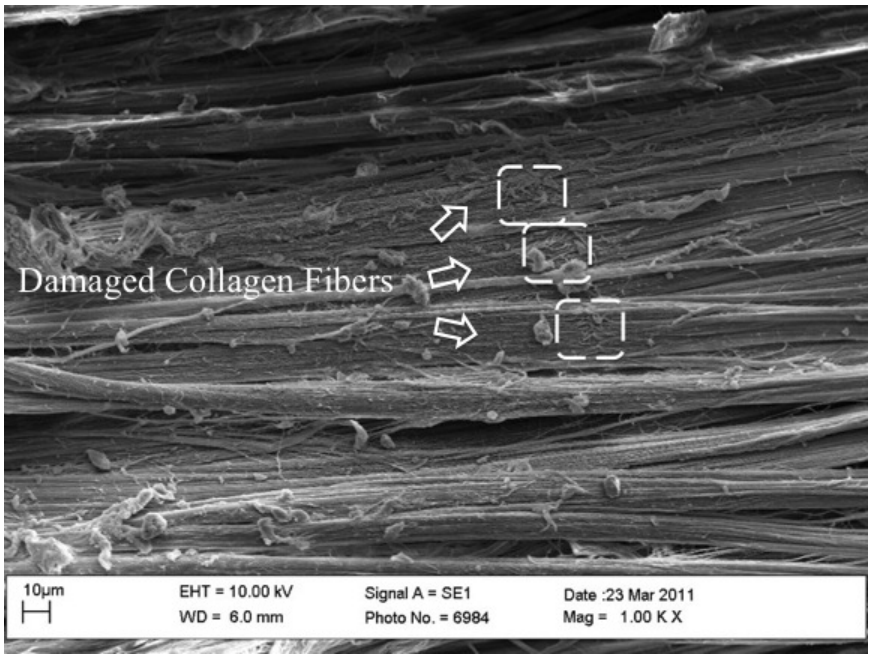

(a) specimen ld_1

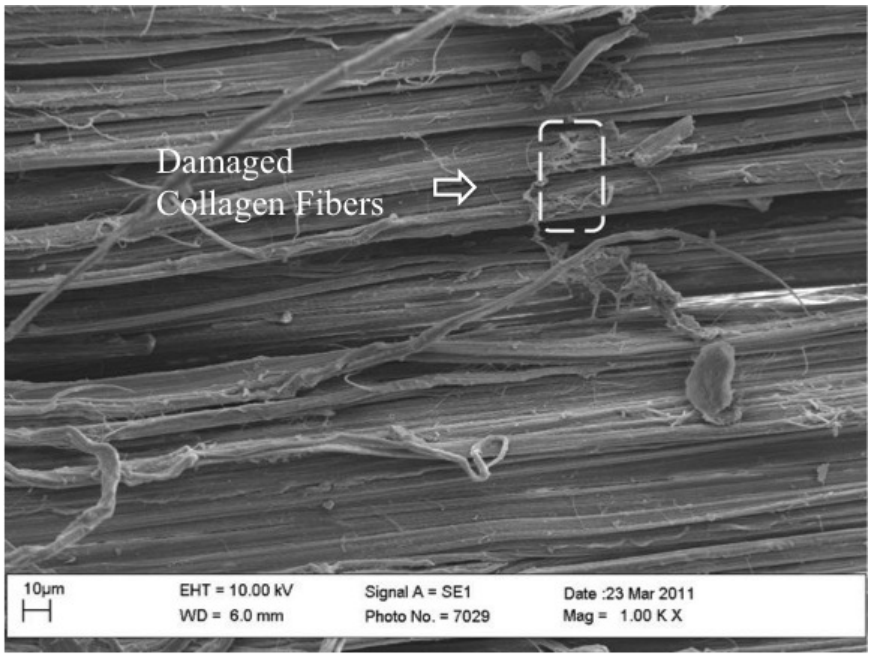

(b) specimen ld_2

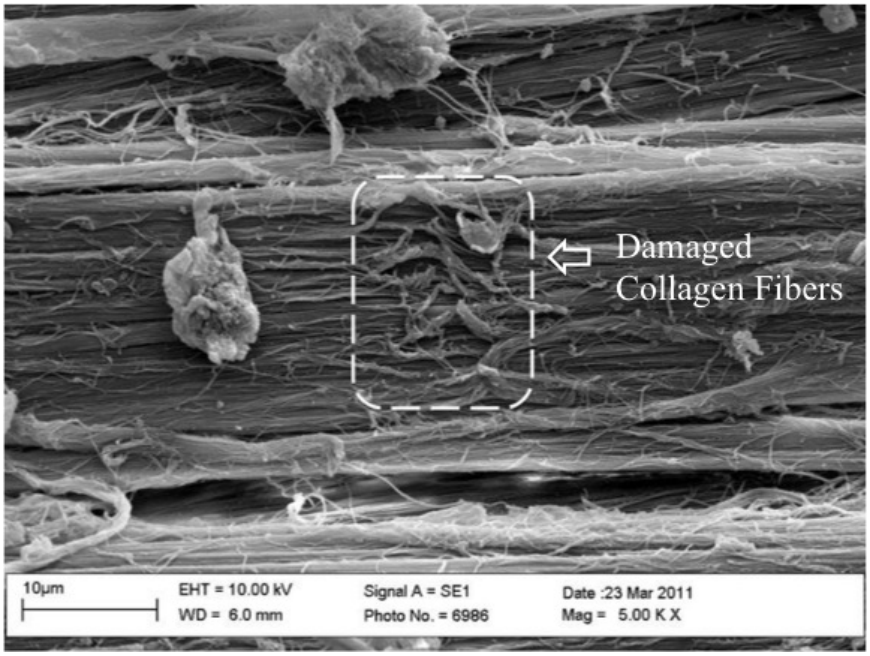

(c) specimen ld_1

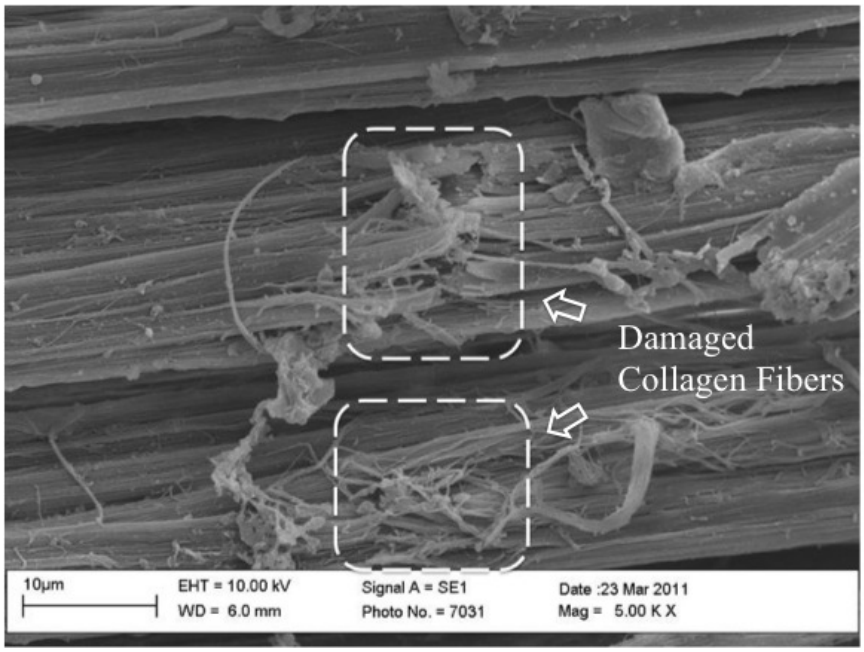

(d) specimen ld_2

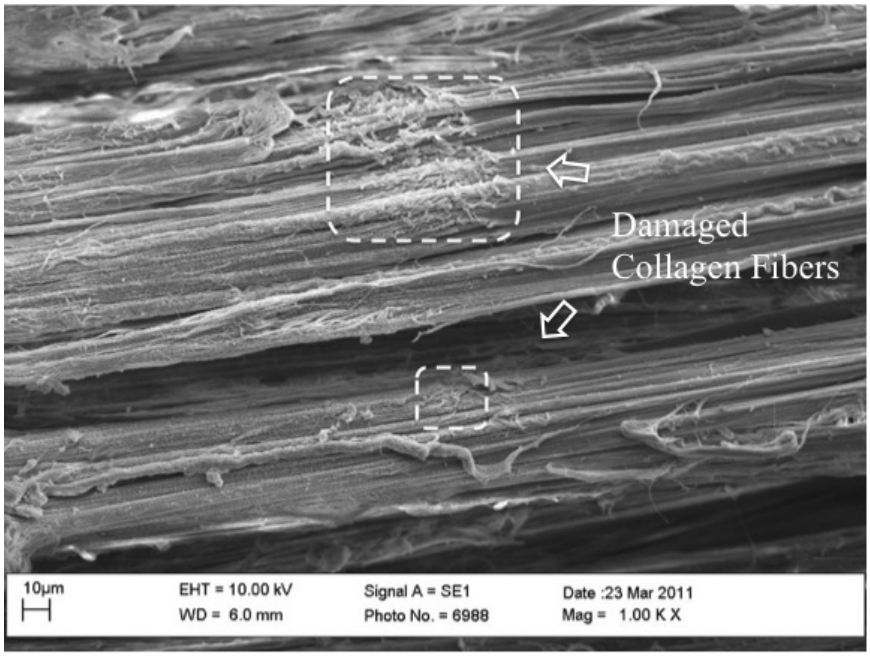

(e) specimen ld_1

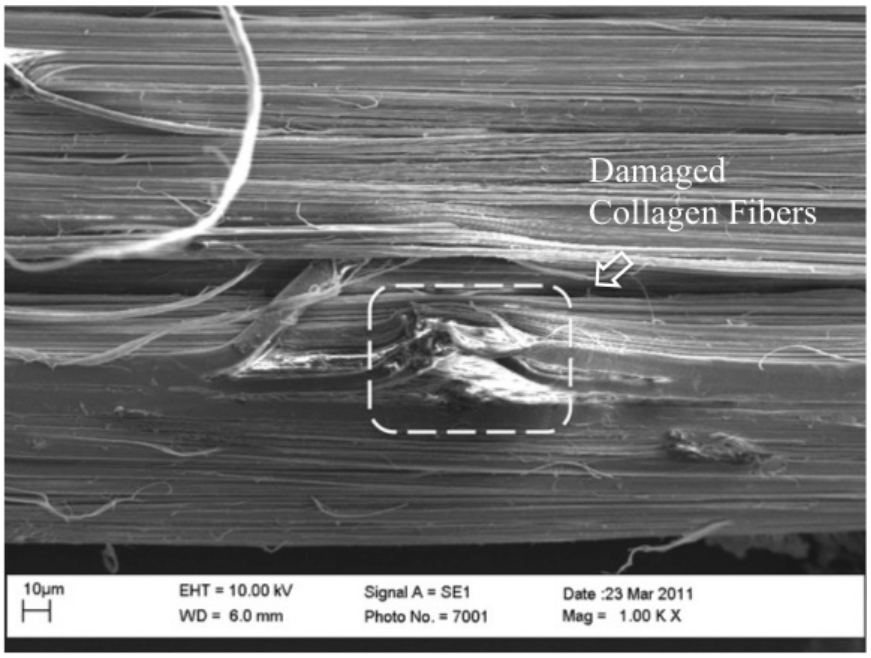

(f) specimen ld_1

Figure 4.8: SEM pictures of MCLs stretched to 0.95 mm (low damaged group) in which the damage to collagen fibers is shown.

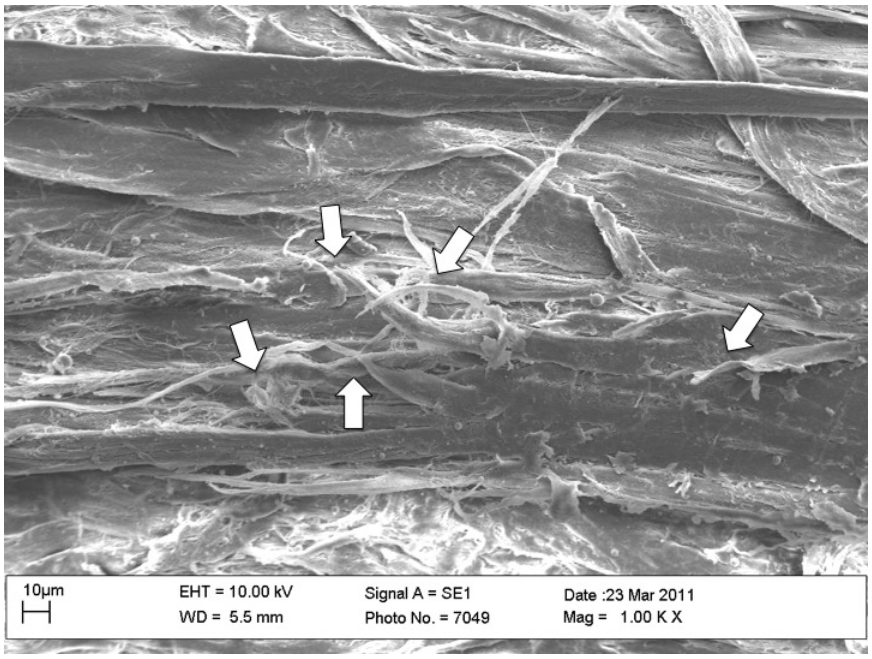

(a) specimen hd_1

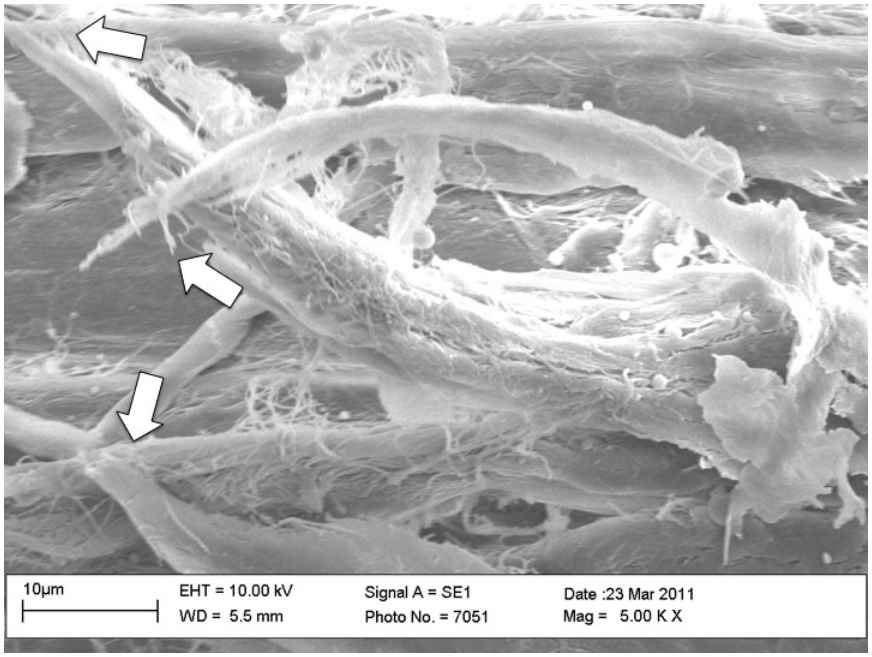

(b) specimen hd_1

Figure 4.9: SEM pictures of MCLs stretched to 1.45 mm (high damaged group) showing broken collagen fibers (arrow).

0.95 mm, which produced strains equal to 3.52% and 4.12%, respectively. Both these strain values exceeded the 2.84% mean value of the threshold strains at which the elongation of the toe region is expected to initiate. The elongation of toe region observed when re-stretching the specimens were calculated to be $\Delta\epsilon_{0.1}^{(2)}$ =0.16% for specimen ld_1 and $\Delta\epsilon_{0.1}^{(2)}$ =0.20% for specimen ld_2. Although the 3.52% and 4.12% applied strains were less than 5.51%, which is the mean value of threshold strains that determines a reduction of tangent modulus in the linear region, some decrease in the tangent modulus of the linear region was noted when re-stretching the specimens ld_1 and ld_2. Specifically, only a slight decrease in the tangent modulus of the linear region ($E^{(2)} = 98.7\%E^{(1)}$) was observed in the specimen ld_2 but a significant decrease in the tangent modulus of the linear region ($E^{(2)} = 85.9\%E^{(1)}$) occurred in specimen ld_1. This decrease in the elastic moduli are due, most probably, to the inability to determine *apriori* the threshold strains for damage due to the variability existing among specimens (see Figure 3.8).

The specimen hd_1 was subjected to a displacement of 1.45 mm, which induced a strain of 6.78%. This strain was greater than the 5.51% that is the mean value of threshold strains at which the tangent modulus of linear region was observed to decrease. A significant decrease in the tangent modulus of the linear region ($E^{(2)} = 87.0\%E^{(1)}$) and an elongation of the toe region were both detected when re-stretching the MCLs.

Microscopic variations associated with the damage observed during mechanical testing were examined under SEM. No significant broken collagen fibers or fibrils were found in the undamaged group (Figure 4.7). A decrease in tangent modulus of the linear region was

recorded when re-stretching the specimens in the low and high damaged groups. In the low damaged group, damage in the collagen fiber was detected as the rupture of collagen fibrils. Because the collagen fibers are major tensile load carriers in ligaments, their damage contributed to the decrease of the tangent modulus of the linear region observed during the second stretching. Specimen ld_1 had more regions in which the collagen fibers appeared damaged (Figure 4.8(a), 4.8(e), 4.8(f)) than specimen ld_2 (Figure 4.8(b)). Consequently, the tangent modulus in the linear region for specimen ld_1 in the second stretching decreased more than that for specimen ld_2 as can be observed in Figure 4.3(a) and Figure 4.3(b).

The elongation of the toe region of the stress-strain curve has been considered an indicator of damage in studies on the effect of monotonic loading/stretching [1, 27, 31] and cyclic loading/stretching [35, 50–52] on ligamentous tissues. It has been speculated that the torn [1, 52] or plastically deformed fibers [1], or damage to the extracellular matrix of ligaments [1, 52] might cause the increase in the elongation of the toe region. The failure of collagen fibers at higher strain levels (as shown in Figure 4.9) is responsible for the tissue's laxity since fewer collagen fibers support the stress in the toe region when re-stretching the ligaments. However, the elongation of the toe region determined by lower strain levels is, perhaps, due to other microscopic damage mechanisms. For instance, for the specimens ld_1 and ld_2, the size of the regions with broken collagen fibrils was different but the elongation of the toe region was similar ($\Delta\epsilon_{0.1}^{(2)}$ =0.16% and 0.20%). This indicates that the breakage of collagen fibrils was not the only factor that produced the elongation of the toe region at low strain levels. Fung et al. [99] observed the morphological changes in flexor digitorum longus tendons after

subfailure damage produced during fatigue tests. The collagen fibers in their studies form kinks under low and moderate level of fatigue. Similarly in this study, it is speculated that the elongation of the toe region maybe be caused by the plastic deformation and formation of kinks in collagen fibers and fibrils observed also in other studies [109–111, 115].

In summary, the microscopic structural changes associated with different levels of subfailure stretches applied to rat MCLs were investigated in order to elucidate the relation between micro-structural and mechanical damage. The waviness of collagen fibrils was different from the waviness of the collagen fiber they form in the slack and preconditioned groups of specimens. The collagen fiber and fibril's waviness gradually disappeared when the ligaments were stretched to increasing displacements. At lower strain levels, neither mechanical damage nor damage to collagen fibers and fibrils were detected. Damage to the collagen fibers represented by the partial failure of their collagen fibrils occurred in the low damaged group of specimens. Complete failure of collagen fibers was only observed in the high damaged specimen. The decrease in the tangent modulus of the linear region of the axial stress-strain curves was speculated to be determined by the fibers' damage or complete failure. The elongation of the toe region was speculated to be caused by the presence of kinks and plastic deformation of collagen fibers and fibrils. Additional SEM studies will be conducted to understand the mechanisms behind the elongation of the toe region of the stress-strain curve in rat MCLs. Damage to the extracellular matrix is also likely to play an important role in the observed mechanical damage phenomena and, hence, need to be also investigated.

Chapter 5

Conclusions and Future Work

In this dissertation, the damage initiation and evolution process in ligaments were studied in order to better understand the etiology of sprains. A structurally based constitutive model was developed to describe the mechanical damage produced by subfailure stretches. The model was able to describe the damage behavior of published rat MCLs [1]. Through mechanical testing of rat MCLs, two damage phenomena, the elongation of the toe region and decrease in tangent modulus of the linear region of ligament's tensile axial stress-strain curve, were observed and quantified. Morphological changes at collagen fiber- and fibril-levels associated with the experimentally observed damage phenomena were investigated by using SEM.

The formulation of the constitutive model was based on the assumption that the tensile load in ligaments is carried only by collagen fibers. The ligament was modeled as a bundle

of wavy collagen fibers orientated along its main loading direction. The contributions of elastin fibers and ground substance were neglected. Moreover, it was assumed that every straight collagen fiber was linear elastic. Damage was determined by the gradual failure of the collagen fibrils that composed the collagen fibers. The gradual recruitment of collagen fibers and the gradual damage of each straight collagen fiber were described by two Weibull distributions. After damage, the elastic modulus of collagen fiber was reduced by a damage factor. The nonlinearities in the toe region and failure region of ligament's tensile axial stress-strain curve were reproduced by the presented model. The model was fit to a published set of experimental data to estimate the model parameters. Using these parameters, the elongation of the toe region and decrease in tangent modulus of the linear region of the stress-strain curves produced by subfailure stretches were successfully predicted. Moreover, it was demonstrated that by changing the parameters in the Weibull distribution that controls the damage process, the model was capable of predicting different failure regions. Finally, the model was used to predict the stress-strain curve of ligaments that received subfailure stretches [1]. However, the predicted stresses were higher than the experimental stresses. These results indicated that other mechanisms that produce damage needed to be incorporated into the model [1].

Tensile tests were performed on Sprague-Dawley rat MCLs. The experimental protocol consisted in monotonically loading the ligaments to incrementally increasing stretches until failure. The non-recoverable changes in ligaments' tensile axial stress-strain curves indicated the occurrence of damage. In addition, MCLs harvested from two age groups of Sprague-

Dawley rats were tested using the same experimental protocol in order to study the effect of age and skeletal maturation on mechanical damage. Two damage phenomena, the elongation of the toe region and decrease in tangent modulus of the linear region, were observed when testing the MCLs. These phenomena were found to occur at two different threshold strains. For MCLs from younger rats, the elongation of the toe region initiates at 2.61±1.33% and the decrease of the tangent modulus of the line initiates at 4.87±1.99%. In MCLs from older rats, the threshold strain that produced an elongation of the toe region was 2.84±1.29% while the threshold strain that produced a decrease in tangent modulus of the linear region was 5.51±2.10%. Statistical analysis showed that the two damage phenomena were determined by significantly different strains ($p<0.05$). However, the effect of age and skeletal maturation on the threshold strains were not statistically significant ($p>0.05$).

SEM analysis was conducted to study the mechanisms that determine the two experimentally observed damage phenomena. Differences in the morphology of collagen fibers and fibrils in normal and damaged ligaments were examined. In the ligaments that received no mechanical stretching or only preconditioning, the collagen fibrils appeared to be more wavy than the collagen fiber they constitute. Moreover, the collagen fibrils tend to form kinks. No microstructure damage was detected in ligaments that were subjected to strains lower than the threshold strains for damage measured in the mechanical experiments. Damage to the collagen fibers, which was detected as partial failure of their fibrils, was observed when stretching the ligaments above the threshold strain that produced the elongation of the toe region. Due to the moderate damage of the collagen fibers, the tangent modulus of the

linear region of the tensile axial stress-strain curve of the ligaments also decreased. The ligaments that were stretched above the threshold strain that was associated with the decrease in tangent modulus of the linear region were observed to have several broken collagen fibers. These results indicated that the decrease in tangent modulus of the linear region is caused by the damage or failure of collagen fibers. Moreover, it was speculated that elongation of the toe region of the stress-strain curve was due to the disappearing of collagen fibrils' kinks or plastic deformation. More studies on the morphological changes of collagen fibrils will be needed to understand the micro-structural mechanisms that lead to the elongation of the toe region.

The results of our research suggest several interesting directions for future work:

1. The presented constitutive model overestimated the stresses in the ligament after damage was introduced by subfailure stretches. The results from the mechanical tests in Chapter 3 showed that the elongation of the toe region and decrease in tangent modulus of the linear region occurred at different threshold strains, which suggested two possible damage mechanisms. Microscopic studies (Chapter 4) also indicated that there are mechanisms other than the failure of collagen fibrils and fibers, considered in the model, which produce the elongation of the toe region. Several studies have shown that cross-links between collagen molecules and collagen fibrils in connective tissues influence their mechanical behavior [91, 116–118]. The breakage of intermolecular and interfibrillar cross-links could be responsible for the damage observed after subfailure stretches and should be included in the model. In the proposed model such damage

could produce an increase in the values of the straightening stretches of collagen fibers and, hence, a more pronounced elongation of the toe region. Moreover, as already mentioned, the ground substance was neglected and the collagen fibers were assumed to have the same orientation. As indicated by Screen et al. [94], the components of the ground substance influence the connective tissues' mechanical properties. Thus, the interaction between collagen fibers or fibrils and the surrounding ground substance need to be considered. Finally, it is worth noticing that the model could be extended to a three-dimensional model by incorporating the description of the collagen fibers's orientation [63, 89].

2. The mechanical tests described in Chapter 3 and 4 were conducted at relatively low displacement rate (0.1 mm/s). It has been reported that when sprains occur in sport and recreational related activities, the strain rates are higher than 50%/s and even reach 150,000%/s [119] (the equivalent displacement rates are 5 mm/s to 15 m/s for the rat ligaments that are approximately 10 mm long). Experimental studies [25–27, 30, 31, 120, 121] conducted on ligaments have shown that the stiffness, elongation at failure and energy absorbed at failure are significantly different at different elongation/loading rates. However, the effect of strain rate (or displacement rate) on the damage evolution process in ligaments still needs further investigation. The experiments conducted in our study at 0.1 mm/s displacement rate should be also conducted at higher displacement rates to better characterize sprains in sports.

3. SEM technique could only provide information about damage that occurred in the two-

dimensional cross-section of the specimens under observation. Imaging techniques, which provide the three-dimensional morphology of ligaments with high resolution, could be used to detect every structural change due to the presence of damage. For example, computer tomography (CT) has been successfully applied to the diagnosis of injuries in ligaments [122–125]. For imaging at micro-scale levels, micro-CT has been developed, which has the capability of obtaining the three-dimensional morphology of the scanning objects with a resolution of approximately 10 μm [126]. Micro-CT has been employed for examining bone tissue [127–130] in order to collect information about its morphological properties. It has been used for obtaining three-dimensional images of several organs and soft tissues. Ritman et al. [131], for example, collected three-dimensional CT images of mouse pulmonary vessels with a resolution of $20\mu m$. Sim et al. [132] obtained the morphology of malleus-incus complex with a resolution of 10-$20\mu m$. Crespigny et al. [133] used micro-CT with a contrast enhanced technique to image the brain and obtained distinct images of its microstructure. These results indicated that the micro-CT technique could provide the needed three-dimensional morphology of damaged ligaments with high resolution and high contrast between different tissues.

Bibliography

[1] P.P. Provenzano, D. Heisey, K. Hayashi, R. Lakes, and R. Vanderby Jr. Subfailure damage in ligament: a structural and cellular evaluation. *Journal of Applied Physiology*, 92(1):362, 2002.

[2] K.C. Miyasaka, D.M. Daniel, M.L. Stone, and P. Hirshman. The incidence of knee ligament injuries in the general population. *American Journal of Knee Surgery*, 4(1):3–8, 1991.

[3] W.J. Warme, J.A. Feagin, P. King, K.L. Lambert, and R.R. Cunningham. Ski injury statistics, 1982 to 1993, Jackson Hole ski resort. *The American Journal of Sports Medicine*, 23(5):597–600, 1995.

[4] L. Peterson, A. Junge, J. Chomiak, T. Graf-Baumann, and J. Dvorak. Incidence of football injuries and complaints in different age groups and skill-level groups. *The American Journal of Sports Medicine*, 28(suppl 5 S-51-S-57), 2000.

[5] B.D. Beynnon, P.A. Renström, D.M. Alosa, J.F. Baumhauer, and P.M. Vacek. An-

kle ligament injury risk factors: a prospective study of college athletes. *Journal of Orthopaedic Research*, 19(2):213–220, 2001.

[6] A.F. Anderson, R.B. Snyder, and A.B. Lipscomb. Anterior cruciate ligament reconstruction. *The American Journal of Sports Medicine*, 29(3):272–279, 2001.

[7] D.M. Daniel, R.A. Pedowitz, O.C. John Joseph, and W.H. Akeson. *Daniel's knee injuries: ligament and cartilage structure, function, injury, and repair*. Lippincott Williams & Wilkins, 2003.

[8] J. Agel, E.A. Arendt, and B. Bershadsky. Anterior cruciate ligament injury in national collegiate athletic association basketball and soccer. *The American Journal of Sports Medicine*, 33(4):524–531, 2005.

[9] P. Phisitkul, S.L. James, B.R. Wolf, and A. Amendola. MCL injuries of the knee: current concepts review. *The Iowa Orthopaedic Journal*, 26:77–90, 2006.

[10] J. Hashemi, N. Chandrashekar, T. Jang, F. Karpat, M. Oseto, and S. Ekwaro-Osire. An alternative mechanism of non-contact anterior cruciate ligament injury during jump-landing: In-vitro simulation. *Experimental Mechanics*, 47(3):347–354, 2007.

[11] P. Rochcongar, E. Laboute, J. Jan, and C. Carling. Ruptures of the anterior cruciate ligament in soccer. *International Journal of Sports Medicine*, 30(5):372–378, 2009.

[12] C.A. Wijdicks, C.J. Griffith, S. Johansen, L. Engebretsen, and R.F. LaPrade. Injuries

to the Medial Collateral Ligament and Associated Medial Structures of the Knee. *The Journal of Bone and Joint Surgery*, 92(5):1266–1280, 2010.

[13] J.M. Hootman, R. Dick, and J. Agel. Epidemiology of collegiate injuries for 15 sports: summary and recommendations for injury prevention initiatives. *Journal of Athletic Training*, 42(2):311, 2007.

[14] J. Webb and I. Corry. Injuries of the sporting knee. *British Medical Journal*, 34(3):227, 2000.

[15] A. Rachun. *Standard nomenclature of athletic injuries*. American Medical Association, 1976.

[16] T. Andriacchi, P. Sabiston, K. De Haven, L. Dahners, S. Woo, C. Frank, B. Oakes, R. Brand, and J. Lewis. Ligament: injury and repair. In S. Y. L. Woo and J. A. Buckwalter, editors, *Injury and Repair of the Musculoskeletal Soft Tissues*. AAOS, Park Ridge, IL, 1987.

[17] S.K. Van de Velde, L.E. DeFrate, T.J. Gill, J.M. Moses, R. Papannagari, and G. Li. The effect of anterior cruciate ligament deficiency on the in vivo elongation of the medial and lateral collateral ligaments. *The American Journal of Sports Medicine*, 35(2):294, 2007.

[18] A. Kanamori, M. Sakane, J. Zeminski, T.W. Rudy, and S.L.Y. Woo. In-situ force in the medial and lateral structures of intact and ACL-deficient knees. *Journal of Orthopaedic Science*, 5(6):567–571, 2000.

[19] K.M. Oates, D.P. Van Eenenaam, K. Briggs, K. Homa, and W.I. Sterett. Comparative injury rates of uninjured, anterior cruciate ligament-deficient, and reconstructed knees in a skiing population. *The American Journal of Sports Medicine*, 27(5):606, 1999.

[20] T.E. Hewett, T.N. Lindenfeld, J.V. Riccobene, and F.R. Noyes. The effect of neuromuscular training on the incidence of knee injury in female athletes. *The American Journal of Sports Medicine*, 27(6):699–706, 1999.

[21] J. Kvist. Rehabilitation following anterior cruciate ligament injury: current recommendations for sports participation. *Sports Medicine*, 34(4):269–280, 2004.

[22] B.M. Nigg and W. Herzog. *Biomechanics of the musculo-skeletal system*. Wiley Chichester, UK, 2007.

[23] M. Nordin and V.H. Frankel. *Basic biomechanics of the musculoskeletal system*. Lippincott Williams & Wilkins, 2001.

[24] C.B. Frank. Ligament structure, physiology and function. *Journal of Musculoskeletal and Neuronal Interactions*, 4(2):199–201, 2004.

[25] S.L.Y. Woo, R.H. Peterson, K.J. Ohland, T.J. Sites, and M.I. Danto. The effects of strain rate on the properties of the medial collateral ligament in skeletally immature and mature rabbits: a biomechanical and histological study. *Journal of Orthopaedic Research*, 8(5):712–721, 1990.

[26] M.I. Danto and S.L.Y. Woo. The mechanical properties of skeletally mature rabbit

anterior cruciate ligament and patellar tendon over a range of strain rates. *Journal of Orthopaedic Research*, 11(1):58–67, 1993.

[27] M.M. Panjabi, E. Yoldas, T.R. Oxland, and J.J. Crisco III. Subfailure injury of the rabbit anterior cruciate ligament. *Journal of Orthopaedic Research*, 14(2):216–222, 1996.

[28] G.M. Thornton, N.G. Shrive, and C.B. Frank. Ligament creep recruits fibres at low stresses and can lead to modulus-reducing fibre damage at higher creep stresses: a study in rabbit medial collateral ligament model. *Journal of Orthopaedic Research*, 20(5):967–974, 2002.

[29] W.R. Su, H.H. Chen, and Z.P. Luo. Effect of cyclic stretching on the tensile properties of patellar tendon and medial collateral ligament in rat. *Clinical Biomechanics*, 23(7):911–917, 2008.

[30] C. Lydon, J.J. Crisco, M. Panjabi, and M. Galloway. Effect of elengation rate on the failure properties of the rabbit anterior cruciate ligament. *Clinical Biomechanics*, 10(8):428–433, 1995.

[31] M.M. Panjabi and T.W. Courtney. High-speed subfailure stretch of rabbit anterior cruciate ligament: changes in elastic, failure and viscoelastic characteristics. *Clinical Biomechanics*, 16(4):334–340, 2001.

[32] R.V. Hingorani, P.P. Provenzano, R.S. Lakes, A. Escarcega, and R. Vanderby. Non-

linear viscoelasticity in rabbit medial collateral ligament. *Annals of Biomedical Engineering*, 32(2):306–312, 2004.

[33] S.L.Y. Woo, R.E. Debski, J.D. Withrow, and M.A. Janaushek. Biomechanics of knee ligaments. *The American Journal of Sports Medicine*, 27(4):533, 1999.

[34] P.P. Provenzano, D.A. Martinez, R.E. Grindeland, K.W. Dwyer, J. Turner, A.C. Vailas, and R. Vanderby Jr. Hindlimb unloading alters ligament healing. *Journal of Applied Physiology*, 94(1):314, 2003.

[35] G.M. Thornton, T.D. Schwab, and T.R. Oxland. Cyclic loading causes faster rupture and strain rate than static loading in medial collateral ligament at high stress. *Clinical Biomechanics*, 22(8):932–940, 2007.

[36] T. Yamaji, R.E. Levine, S.L.Y. Woo, C. Niyibizi, K.W. Kavalkovich, and C.M. Weaver-Green. Medial collateral ligament healing one year after a concurrent medial collateral ligament and anterior cruciate ligament injury: An interdisciplinary study in rabbits. *Journal of Orthopaedic Research*, 14(2):223–227, 1996.

[37] M. Noguchi, T. Kitaura, K. Ikoma, and Y. Kusaka. A method of in-vitro measurement of the cross-sectional area of soft tissues, using ultrasonography. *Journal of Orthopaedic Science*, 7(2):247–251, 2002.

[38] D.K. Moon, S.D. Abramowitch, and S.L.Y. Woo. The development and validation of a charge-coupled device laser reflectance system to measure the complex cross-sectional shape and area of soft tissues. *Journal of Biomechanics*, 39(16):3071–3075, 2006.

[39] S.T. Salisbury, C.P. Buckley, and A.B. Zavatsky. Image-based non-contact method to measure cross-sectional areas and shapes of tendons and ligaments. *Measurement Science and Technology*, 19:045705, 2008.

[40] J.C. Kennedy, R.J. Hawkins, and R.B. Willis. Strain gauge analysis of knee ligaments. *Clinical Orthopaedics and Related Research*, 129:225, 1977.

[41] G.S. Berns, ML Hull, and H.A. Patterson. Strain in the anteromedial bundle of the anterior cruciate ligament under combination loading. *Journal of Orthopaedic Research*, 10(2):167–176, 1992.

[42] J.M. Bach, M.L. Hull, and H.A. Patterson. Direct measurement of strain in the posterolateral bundle of the anterior cruciate ligament. *Journal of Biomechanics*, 30(3):281–283, 1997.

[43] B. Beynnon, JG Howe, M.H. Pope, R.J. Johnson, and B.C. Fleming. The measurement of anterior cruciate ligament strain in vivo. *International Orthopaedics*, 16(1):1–12, 1992.

[44] B.C. Fleming, B.D. Beynnon, H. Tohyama, R.J. Johnson, C.E. Nichols, P. Renström, and M.H. Pope. Determination of a zero strain reference for the anteromedial band of the anterior cruciate ligament. *Journal of Orthopaedic Research*, 12(6):789–795, 1994.

[45] K.M. Quapp and J.A. Weiss. Material characterization of human medial collateral ligament. *Journal of Biomechanical Engineering*, 120:757, 1998.

[46] C.M. Tipton, R.D. Matthes, and R.K. Martin. Influence of age and sex on the strength of bone-ligament junctions in knee joints of rats. *The Journal of Bone and Joint Surgery*, 60(2):230–234, 1978.

[47] Y. Gijssen, I.N. Sierevelt, J.G.M. Kooloos, and L. Blankevoort. Stiffness of the healing medial collateral ligament of the mouse. *Connective Tissue Research*, 45(3):190–195, 2004.

[48] S.L.Y. Woo, K.J. Ohland, and J.A. Weiss. Aging and sex-related changes in the biomechanical properties of the rabbit medial collateral ligament. *Mechanisms of Ageing and Development*, 56(2):129–142, 1990.

[49] S.L.Y. Woo, C.A. Orlando, M.A. Gomez, C.B. Frank, and W.H. Akeson. Tensile properties of the medial collateral ligament as a function of age. *Journal of Orthopaedic Research*, 4(2):133–141, 1986.

[50] G.J.W. King, C.L. Pillon, and J.A. Johnson. Effect of in vitro testing over extended periods on the low-load mechanical behaviour of dense connective tissues. *Journal of Orthopaedic Research*, 18(4):678–681, 2000.

[51] R.G. Pollock, V.M. Wang, J.S. Bucchieri, N.P. Cohen, C.Y. Huang, R.J. Pawluk, E.L. Flatow, L.U. Biqilani, and V.C. Mow. Effects of repetitive subfailure strains on the mechanical behavior of the inferior glenohumeral ligament. *Journal of Shoulder and Elbow Surgery*, 9(5):427–435, 2000.

[52] G.M. Thornton, T.D. Schwab, and T.R. Oxland. Fatigue is more damaging than creep in ligament revealed by modulus reduction and residual strength. *Annals of Biomedical Engineering*, 35(10):1713–1721, 2007.

[53] M.L. Zec, P. Thistlethwaite, C.B. Frank, and N.G. Shrive. Characterization of the fatigue behavior of the medial collateral ligament utilizing traditional and novel mechanical variables for the assessment of damage accumulation. *Journal of Biomechanical Engineering*, 132(1):011001, 2010.

[54] G. Laws and M. Walton. Fibroblastic healing of grade II ligament injuries. Histological and mechanical studies in the sheep. *Journal of Bone and Joint Surgery, British Volume*, 70(3):390–396, 1988.

[55] K.E. Lee, A.N. Franklin, M.B. Davis, and B.A. Winkelstein. Tensile cervical facet capsule ligament mechanics: failure and subfailure responses in the rat. *Journal of Biomechanics*, 39(7):1256–1264, 2006.

[56] K.P. Quinn and B.A. Winkelstein. Altered collagen fiber kinematics define the onset of localized ligament damage during loading. *Journal of Applied Physiology*, 105(6):1881–1888, 2008.

[57] K.P. Quinn and B.A. Winkelstein. Vector correlation technique for pixel-wise detection of collagen fiber realignment during injurious tensile loading. *Journal of Biomedical Optics*, 14(5):054010, 2009.

[58] M.K. Kwan and S.L.Y. Woo. A structural model to describe the nonlinear stress-strain behavior for parallel-fibered collagenous tissues. *Journal of Biomechanical Engineering*, 111(4):361–363, 1989.

[59] C. Hurschler, B. Loitz-Ramage, and R. Vanderby Jr. A structurally based stress-stretch relationship for tendon and ligament. *Journal of Biomechanical Engineering*, 119(4):392–399, 1997.

[60] C. Hurschler, P.P. Provenzano, and R. Vanderby Jr. Application of a probabilistic microstructural model to determine reference length and toe-to-linear region transition in fibrous connective tissue. *Journal of Biomechanical Engineering*, 125(3):415–422, 2003.

[61] T.A.L. Wren and D.R. Carter. A microstructural model for the tensile constitutive and failure behavior of soft skeletal connective tissues. *Journal of Biomechanical Engineering*, 120(1):55–61, 1998.

[62] H. Liao and S.M. Belkoff. A failure model for ligaments. *Journal of Biomechanics*, 32(2):183–188, 1999.

[63] R. De Vita and W.S. Slaughter. A constitutive law for the failure behavior of medial collateral ligaments. *Biomechanics and Modeling in Mechanobiology*, 6(3):189–197, 2007.

[64] J.F. Rodríguez, F. Cacho, J.A. Bea, and M. Doblaré. A stochastic-structurally based

three dimensional finite-strain damage model for fibrous soft tissue. *Journal of the Mechanics and Physics of Solids*, 54(4):864–886, 2006.

[65] J.F. Rodríguez, V. Alastrue, and M. Doblare. Finite element implementation of a stochastic three dimensional finite-strain damage model for fibrous soft tissue. *Computer Methods in Applied Mechanics and Engineering*, 197(9-12):946–958, 2008.

[66] P.J. Arnoux, P. Chabrand, M. Jean, and J. Bonnoit. A visco-hyperelastic model with damage for the knee ligaments under dynamic constraints. *Computer Methods in Biomechanics and Biomedical Engineering*, 5(2):167–174, 2002.

[67] E. Peña, MA Martínez, B. Calvo, and M. Doblaré. Application of the natural element method to finite deformation inelastic problems in isotropic and fiber-reinforced biological soft tissues. *Computer Methods in Applied Mechanics and Engineering*, 197(21-24):1983–1996, 2008.

[68] T.D. Schwab, C.R. Johnston, T.R. Oxland, and G.M. Thornton. Continuum damage mechanics (CDM) modelling demonstrates that ligament fatigue damage accumulates by different mechanisms than creep damage. *Journal of Biomechanics*, 40(14):3279–3284, 2007.

[69] A.N. Natali, E.L. Carniel, P.G. Pavan, F.G. Sander, C. Dorow, and M. Geiger. A visco-hyperelastic-damage constitutive model for the analysis of the biomechanical response of the periodontal ligament. *Journal of Biomechanical Engineering*, 130(3):031004, 2008.

[70] P. Ciarletta and M. Ben Amar. A finite dissipative theory of temporary interfibrillar bridges in the extracellular matrix of ligaments and tendons. *Journal of The Royal Society Interface*, 6(39):909–924, 2008.

[71] B. Calvo, E. Peña, MA Martínez, and M. Doblaré. An uncoupled directional damage model for fibred biological soft tissues. Formulation and computational aspects. *International Journal for Numerical Methods in Engineering*, 69(10):2036–2057, 2007.

[72] A.N. Natali, P.G. Pavan, E.L. Carniel, M.E. Lucisano, and G. Taglialavoro. Anisotropic elasto-damage constitutive model for the biomechanical analysis of tendons. *Medical Engineering & Physics*, 27(3):209–214, 2005.

[73] Z. Guo and R. De Vita. Probabilistic constitutive law for damage in ligaments. *Medical engineering & physics*, 31(9):1104–1109, 2009.

[74] D. Amiel, E. Billings, and W.H. Akeson. Ligament structure, chemistry, and physiology. In Daniel D., Akeson W., and O'Connor J., editors, *Knee ligaments: structure, function, injury and repair*. Raven Press, New York, NY, 1990.

[75] J. Kastelic, A. Galeski, and E. Baer. The multicomposite structure of tendon. *Connective tissue research*, 6(1):11–23, 1978.

[76] K.A. Hansen, J.A. Weiss, and J.K. Barton. Recruitment of tendon crimp with applied tensile strain. *Journal of Biomechanical Engineering*, 124:72–77, 2002.

[77] N. Sasaki and S. Odajima. Stress-strain curve and Young's modulus of a collagen

molecule as determined by the X-ray diffraction technique. *Journal of Biomechanics*, 29(5):655–658, 1996.

[78] W.J. Weibull. A statistical distribution function of wide applicability. *Journal of Applied Mechanics*, 18:293–297, 1951.

[79] S.K. Park and K.W. Miller. Random number generators: good ones are hard to find. *Communications of the ACM*, 31(10):1192–1201, 1988.

[80] W.H. Press, B.P. Flannery, S.A. Teukolsky, and W.T. Vetterling. *Numerical recipes in C: the art of scientific computing*. Cambridge University Press New York, NY, USA, 1992.

[81] K.V. Price, R.M. Storn, and J.A. Lampinen. *Differential evolution: a practical approach to global optimization*. Springer Verlag, 2005.

[82] H.E. Daniels. The statistical theory of the strength of bundles of threads. I. *Proceedings of the Royal Society of London. Series A. Mathematical and Physical Sciences*, 183(995):405, 1945.

[83] L.N. McCartney and R.L. Smith. Statistical theory of the strength of fiber bundles. *Journal of Applied Mechanics*, 50:601, 1983.

[84] L. Mishnaevsky Jr and P. Brøndsted. Micromechanical modeling of damage and fracture of unidirectional fiber reinforced composites: A review. *Computational Materials Science*, 44(4):1351–1359, 2009.

[85] F. Kun, S. Zapperi, and H.J. Herrmann. Damage in fiber bundle models. *The European Physical Journal B-Condensed Matter and Complex Systems*, 17(2):269–279, 2000.

[86] R.C. Hidalgo, F. Kun, and H.J. Herrmann. Bursts in a fiber bundle model with continuous damage. *Physical Review E*, 64(6):066122, 2001.

[87] J.A. Weiss and J.C. Gardiner. Computational modeling of ligament mechanics. *Critical Reviews in Biomedical Engineering*, 29(4):1–70, 2001.

[88] Y. Lanir. A structural theory for the homogeneous biaxial stress-strain relationships in flat collagenous tissues. *Journal of Biomechanics*, 12(6):423–436, 1979.

[89] R. De Vita and W.S. Slaughter. A structural constitutive model for the strain rate-dependent behavior of anterior cruciate ligaments. *International Journal of Solids and Structures*, 43(6):1561–1570, 2006.

[90] A.J. Bailey, S.P. Robins, and G. Balian. Biological significance of the intermolecular crosslinks of collagen. *Nature*, 251:105–109, 1974.

[91] P. Fratzl, K. Misof, and I. ZizakGert. Fibrillar structure and mechanical properties of collagen. *Journal of structural biology*, 122(1-2):119–122, 1998.

[92] R.J. Minns, P.D. Soden, and D.S. Jackson. The role of the fibrous components and ground substance in the mechanical properties of biological tissues: a preliminary investigation. *Journal of Biomechanics*, 6(2):153–165, 1973.

[93] H.R.C. Screen, D.A. Lee, D.L. Bader, and J.C. Shelton. An investigation into the effects of the hierarchical structure of tendon fascicles on micromechanical properties. *Proceedings of the Institution of Mechanical Engineers, Part H: Journal of Engineering in Medicine*, 218(2):109–119, 2004.

[94] H.R.C. Screen, J.C. Shelton, V.H. Chhaya, M.V. Kayser, D.L. Bader, and D.A. Lee. The influence of noncollagenous matrix components on the micromechanical environment of tendon fascicles. *Annals of Biomedical Engineering*, 33(8):1090–1099, 2005.

[95] S.L.Y. Woo, S.D. Abramowitch, R. Kilger, and R. Liang. Biomechanics of knee ligaments: injury, healing, and repair. *Journal of Biomechanics*, 39(1):1–20, 2006.

[96] X.T. Wang, R.F. Ker, and R.M. Alexander. Fatigue rupture of wallaby tail tendons. *The Journal of Experimental Biology*, 198(Pt 3):847–852, 1995.

[97] H. Schechtman and D.L. Bader. Fatigue damage of human tendons. *Journal of Biomechanics*, 35(3):347–353, 2002.

[98] T.A.L. Wren, D.P. Lindsey, G.S. Beaupre, and D.R. Carter. Effects of creep and cyclic loading on the mechanical properties and failure of human Achilles tendons. *Annals of Biomedical Engineering*, 31(6):710–717, 2003.

[99] D.T. Fung, V.M. Wang, D.M. Laudier, J.H. Shine, J. Basta-Pljakic, K.J. Jepsen, M.B. Schaffler, and E.L. Flatow. Subrupture tendon fatigue damage. *Journal of Orthopaedic Research*, 27(2):264–273, 2009.

[100] M.M. Panjabi, R.C. Huang, and J. Cholewicki. Equivalence of single and incremental subfailure stretches of rabbit anterior cruciate ligament. *Journal of Orthopaedic Research*, 18(5):841–848, 2000.

[101] P. Blæsild and J. Granfeldt. *Statistics with applications in biology and geology*. Chapman & Hall/CRC, 2003.

[102] A. Viidik. A rheological model for uncalcified parallel-fibred collagenous tissue. *Journal of Biomechanics*, 1(1):3–11, 1968.

[103] X. Wei and K. Messner. The postnatal development of the insertions of the medial collateral ligament in the rat knee. *Anatomy and Embryology*, 193(1):53–59, 1996.

[104] S.L.Y. Woo, M.A. Gomez, Y. Seguchi, C.M. Endo, and W.H. Akeson. Measurement of mechanical properties of ligament substance from a bone-ligament-bone preparation. *Journal of Orthopaedic Research*, 1(1):22–29, 1983.

[105] Y. Fung. *Biomechanics: mechanical properties of living tissues*. Springer, 1993.

[106] C. Frank, B. MacFarlane, P. Edwards, R. Rangayyan, Z.Q. Liu, S. Walsh, and R. Bray. A quantitative analysis of matrix alignment in ligament scars: a comparison of movement versus immobilization in an immature rabbit model. *Journal of Orthopaedic Research*, 9(2):219–227, 1991.

[107] C. Hurschler, P.P. Provenzano, and R. Vanderby. Scanning electron microscopic char-

acterization of healing and normal rat ligament microstructure under slack and loaded conditions. *Connective Tissue Research*, 44(2):59–68, 2003.

[108] P.P. Provenzano, R. Vanderby, et al. Collagen fibril morphology and organization: implications for force transmission in ligament and tendon. *Matrix biology*, 25(2):71–84, 2006.

[109] M. Raspanti, A. Manelli, M. Franchi, and A. Ruggeri. The 3D structure of crimps in the rat Achilles tendon. *Matrix biology*, 24(7):503–507, 2005.

[110] M. Franchi, M. Fini, M. Quaranta, V. De Pasquale, M. Raspanti, G. Giavaresi, V. Ottani, and A. Ruggeri. Crimp morphology in relaxed and stretched rat Achilles tendon. *Journal of Anatomy*, 210(1):1–7, 2007.

[111] M. Franchi, V. Ottani, R. Stagni, and A. Ruggeri. Tendon and ligament fibrillar crimps give rise to left-handed helices of collagen fibrils in both planar and helical crimps. *Journal of Anatomy*, 216(3):301–309, 2010.

[112] L. Yahia, J. Brunet, S. Labelle, and CH Rivard. A scanning electron microscopic study of rabbit ligaments under strain. *Matrix (Stuttgart, Germany)*, 10(1):58, 1990.

[113] P.P. Provenzano, A.L. Alejandro-Osorio, W.B. Valhmu, K.T. Jensen, R. Vanderby, et al. Intrinsic fibroblast-mediated remodeling of damaged collagenous matrices in vivo. *Matrix Biology*, 23(8):543–555, 2005.

[114] S.D. Dodds, M.M. Panjabi, and J.P. Daigneault. Radiofrequency probe treatment for

subfailure ligament injury: a biomechanical study of rabbit ACL. *Clinical Biomechanics*, 19(2):175–183, 2004.

[115] T. Gutsmann, G.E. Fantner, M. Venturoni, A. Ekani-Nkodo, J.B. Thompson, J.H. Kindt, D.E. Morse, D.K. Fygenson, and P.K. Hansma. Evidence that collagen fibrils in tendons are inhomogeneously structured in a tubelike manner. *Biophysical Journal*, 84(4):2593–2598, 2003.

[116] K. Misof, G. Rapp, and P. Fratzl. A new molecular model for collagen elasticity based on synchrotron X-ray scattering evidence. *Biophysical Journal*, 72(3):1376–1381, 1997.

[117] R. Puxkandl, I. Zizak, O. Paris, J. Keckes, W. Tesch, S. Bernstorff, P. Purslow, and P. Fratzl. Viscoelastic properties of collagen: synchrotron radiation investigations and structural model. *Philosophical Transactions of the Royal Society of London. Series B: Biological Sciences*, 357(1418):191, 2002.

[118] T. Gutsmann, G.E. Fantner, J.H. Kindt, M. Venturoni, S. Danielsen, and P.K. Hansma. Force spectroscopy of collagen fibers to investigate their mechanical properties and structural organization. *Biophysical Journal*, 86(5):3186–3193, 2004.

[119] R.D. Crowninshield and M.H. Pope. The strength and failure characteristics of rat medial collateral ligaments. *The Journal of Trauma*, 16(2):99, 1976.

[120] D.P. Pioletti, L.R. Rakotomanana, and P.F. Leyvraz. Strain rate effect on the mechanical behavior of the anterior cruciate ligament- bone complex. *Medical Engineering & Physics*, 21(2):95–100, 1999.

[121] J.J. Crisco, D.C. Moore, and R.D. McGovern. Strain-rate sensitivity of the rabbit MCL diminishes at traumatic loading rates. *Journal of Biomechanics*, 35(10):1379–1385, 2002.

[122] A.I. Bloom, Z. Neeman, B. Simon Slasky, Y. Floman, M. Milgrom, A. Rivkind, and J. Bar-Ziv. Fracture of the occipital condyles and associated craniocervical ligament injury: incidence, CT imaging and implications. *Clinical Radiology*, 52(3):198–202, 1997.

[123] B.C. Vande Berg, F.E. Lecouvet, P. Poilvache, J.E. Dubuc, B. Maldague, and J. Malghem. Anterior cruciate ligament tears and associated meniscal lesions: assessment at dual-detector spiral CT arthrography. *Radiology*, 223(2):403–409, 2002.

[124] M.R. Schmid, T. Schertler, C.W. Pfirrmann, N. Saupe, M. Manestar, S. Wildermuth, and D. Weishaupt. Interosseous ligament tears of the wrist: comparison of multi–detector row CT arthrography and MR imaging. *Radiology*, 237(3):1008–1013, 2005.

[125] L.W. Mui, E. Engelsohn, and H. Umans. Comparison of CT and MRI in patients with tibial plateau fracture: can CT findings predict ligament tear or meniscal injury? *Skeletal Radiology*, 36(2):145–151, 2007.

[126] E.L. Ritman. Micro-computed tomography:current status and developments. *Annual Review of Biomedical Engineering*, 6(1):185–208, 2004.

[127] B. Borah, G.J. Gross, T.E. Dufresne, T.S. Smith, M.D. Cockman, P.A. Chmielewski, M.W. Lundy, J.R. Hartke, and E.W. Sod. Three-dimensional microimaging (MRmicroI

and microCT), finite element modeling, and rapid prototyping provide unique insights into bone architecture in osteoporosis. *The Anatomical Record*, 265(2):101–110, 2001.

[128] S. Judex, S. Boyd, Y.X. Qin, L. Miller, R. Müller, and C. Rubin. Combining high-resolution micro-computed tomography with material composition to define the quality of bone tissue. *Current Osteoporosis Reports*, 1(1):11–19, 2003.

[129] D.L. Batiste, A. Kirkley, S. Laverty, L.M.F. Thain, A.R. Spouge, J.S. Gati, P.J. Foster, and D.W. Holdsworth. High-resolution MRI and micro-CT in an ex vivo rabbit anterior cruciate ligament transection model of osteoarthritis. *Osteoarthritis and Cartilage*, 12(8):614–626, 2004.

[130] F.W. Roemer, A. Mohr, J.A. Lynch, M.D. Meta, A. Guermazi, and H.K. Genant. Micro-CT arthrography: A pilot study for the ex vivo visualization of the rat knee joint. *American Journal of Roentgenology*, 184(4):1215–1219, 2005.

[131] E.L. Ritman. Micro-computed tomography of the lungs and pulmonary-vascular system. In *Proceedings of the American Thoraic Society*, volume 2, pages 477–480. American Thoracic Society, 2005.

[132] J.H. Sim and S. Puria. Soft Tissue Morphometry of the Malleus–Incus Complex from Micro-CT Imaging. *JARO - Journal of the Association for Research in Otolaryngology*, 9(1):5–21, 2008.

[133] A. de Crespigny, H. Bou-Reslan, M.C. Nishimura, H. Phillips, R.A.D. Carano, and H.E.

D'Arceuil. 3D micro-CT imaging of the postmortem brain. *Journal of Neuroscience Methods*, 171(2):207–213, 2008.